Biophysical Journal Volume 71 October 1996 1934–1951

Spectral Broadening of Interacting Pigments: Polarized Absorption by Photosynthetic Proteins

Oscar J. G. Somsen, Rienk van Grondelle, and Herbert van Amerongen
Department of Physics and Astronomy, Free University Amsterdam, 1081 HV Amsterdam, The Netherlands

ABSTRACT Excitonic interaction between pigment molecules is largely responsible for the static and dynamic spectroscopic properties of photosynthetic pigment-proteins. This paper provides a new description of its effect on polarized absorption spectroscopy, in particular on circular dichroism (CD). We investigate excitonic spectra of finite width and use "spectral moments" to compare 1) inhomogeneously broadened excitonic spectra, 2) spectra that are (homogeneously) broadened by vibrations or electron-phonon interaction, and 3) spectra that are simulated by applying convolution after the interaction has been evaluated. Two cases are distinguished. If the excitonic splitting is smaller than the width of the interacting absorption bands, the broadening of the excitonic spectrum can be approximated by a convolution approach, although a correction is necessary for CD spectra. If the excitonic splitting exceeds the bandwidth, the well-known exchange narrowing occurs. We demonstrate that this is accompanied by redistribution of dipole strength and spectral shifts. The magnitude of a CD spectrum is conveniently expressed by its first spectral moment. As will be shown, this is independent of spectral broadening as well as dispersive shifts induced by pigment-protein interactions. Consequently, it provides a simple tool to relate the experimental CD spectrum of a pigment complex to the excitonic interactions from which it originates. To illustrate the potential of the presented framework, the spectroscopy of the LH2 pigment-protein complex from purple bacteria is analyzed and compared for dimer-like and ring-like structures. Furthermore, it is demonstrated that the variability of the CD of chlorosomes from green bacteria can be explained by small changes in the structure of their cylindrical bacteriochlorophyll *c* subunits.

INTRODUCTION

Chlorophyll pigments are the main cofactors in photosynthetic proteins. In the light-harvesting antenna they are responsible for light absorption and transport of excitation energy. In the reaction center they also participate in electron transfer. The spectroscopic properties of the antenna pigments differ considerably from those of pigments in solution as a result of interactions with their environment. In this paper we consider steady-state polarized absorption spectra, which are easy to measure and potentially very sensitive to these short-range interactions.

Two types of interactions are to be distinguished. First, pigment-pigment interactions induce mixing of the excited states of different pigments and lead to excitonic splitting of the absorption spectrum into a new set of transitions. Second, pigment-protein interactions, caused by charge or polarizability of amino acids and hydrogen bonds, affect the properties of individual pigments, such as dispersive shifts of their absorption bands. In addition, the protein has a strong effect on the widths of the absorption bands. It provides a glass-like medium that causes inhomogeneous broadening, whereas further broadening results from phonons in the protein that couple to the electronic states of the pigment (see, for instance, Jankowiak et al., 1993). In this paper we refer to the latter mechanism as homogeneous broadening and distinguish it from broadening that is related to dephasing and excited state decay.

For a detailed study of broadened excitonic spectra, the effects of pigment-pigment and pigment-protein interaction should be considered simultaneously. This causes special features, such as exchange narrowing. As we will demonstrate, it can also be partially responsible for the appearance of unexpected shoulders and the asymmetry of spectral bands.

Circular dichroism

Two types of spectra are emphasized in this paper. First, absorption (OD) spectra give a global indication of the positions of the excitonic transitions and of the magnitude of the spectral broadening. In most photosynthetic bacteria, the near infrared spectrum is characterized by a large red shift with respect to bacteriochlorophyll (Bchl) in solution. The excitonic transitions are rarely observed as separate bands. This is due to overlap and unequal distribution of dipole strengths. In the antenna proteins of photosynthetic purple bacteria, only one band is observed for each pigment pool, whereas a set of strongly overlapping bands is typically observed for more complex proteins such as the Fenna-Matthews-Olson (FMO) complex (Pearlstein, 1991) and the LHCII complex (Nussberger et al., 1994).

Additional information about excitonic interaction can be obtained from circular dichroism (CD), defined as the difference in absorption of left and right circularly polarized

Received for publication 13 November 1995 and in final form 17 June 1996.

Address reprint requests to Dr. Herbert van Amerongen, Department of Physics and Astronomy, Free University Amsterdam, De Boelelaan 1081, 1081 HV Amsterdam, The Netherlands. Tel.: 31-20-4447932; Fax: 31-20-4447899; E-mail: herbert@nat.vu.nl.

0006-3495/96/10/1934/18 $2.00

light. This can be both positive and negative, and the characteristic S-shaped spectra that are observed in light-harvesting complexes of photosynthetic purple bacteria (Visschers et al., 1991; Kramer et al., 1984) are a strong indication of the presence of more than one excitonic transition within the absorption band. These CD spectra are often, but not always, nearly conservative, i.e., the areas of the positive and negative lobes are equal. Larger and less symmetric photosynthetic proteins such as the FMO complex (Pearlstein, 1991) and the LHCII complex (Nussberger et al., 1994) show more complicated CD spectra, which can only approximately be described as a sum of such S-shaped spectra. Moreover, the latter has a strongly nonconservative character, indicating that not only Q_y-Q_y interactions are important. On the other hand, the CD of the very large, highly symmetrical chlorophyll aggregates in chlorosomes is more or less conservative and has been proposed to be a sum of two somewhat asymmetric S-shaped spectra (Griebenow et al., 1991). The relative contributions of these two spectra vary between samples.

In this paper, we will not explicitly discuss linear dichroism (LD), which is observed in partially oriented samples, although it can be described with the same approach. For a better understanding of excitonic interaction within a pigment-protein complex, LD and CD spectra may, however, be considered together and in concert with other techniques such as fluorescence and transient absorption spectra.

Previous studies on excitonic spectra

Many studies have been published on the theory of excitonic spectra of photosynthetic proteins (for a review see Pearlstein, 1991). Three major steps can be distinguished and the various studies can be differentiated by the approximations in each step. In the first step, the electronic interaction strengths are estimated from a structural model and combined in the Hamiltonian of the complex. In the second step, the new set of excitonic eigenstates of the Hamiltonian is obtained. The transitions between these states form the so-called excitonic stick spectrum. Finally, spectral broadening is applied to the excitonic transitions to form bands of finite width.

Before outlining the approach in this paper, let us first consider the possible approximations in each step. The evaluation of electronic interactions requires a charge distribution operator and its expectation and transition values. These are approximated by dipole moments, as long as net charges are absent and the pigments are smaller than the distance between them. More general is the Point Charge Model (PCM). This was applied to simplified Bchl models by LaLonde et al. (1988, 1989 and references therein). These authors found considerable differences between the PCM and dipole-dipole interaction for center-to-center distances below 0.9 nm. Extended dipoles (Pearlstein, 1991), formed by opposite charges at a finite distance, may serve as an intermediate between these two approaches.

In the second step, the new excitonic eigen states are formed by mixing states of the individual pigments. The simplest models (Fidder et al., 1991; Alden et al., 1992; Pearlstein, 1991) include one excited state for each pigment, corresponding to the absorption band under consideration. This may be improved for chlorophyll (Chl) (Scherz et al., 1991; LaLonde et al., 1988), because at least four excited states are known (Q_y, Q_x, B_x, and B_y). In many cases, however, the interaction with these other states is weak, i.e., small with respect to the energetic separation between them, and may be ignored. For example, the Q_y and Q_x transitions of Bchl *a* are separated by 4000 cm^{-1}, whereas the interaction between two pigments at 1 nm distance does not exceed 400 cm^{-1}. Nevertheless, it may be necessary to include these or even charge transfer states (Warshel and Parson, 1987) to explain particular phenomena, such as hyper- and hypochromism and nonconservative CD, because these do not occur for interaction within a spectral band. This can often be done with a first-order perturbation approach.

In the final step, to obtain the excitonic spectrum, the finite width of the absorption bands must be considered. If the bandwidth of the monomer spectrum is less than the excitonic splitting, each transition in the excitonic spectrum is replaced by a band of finite width. Exchange narrowing occurs in these spectra (Förster, 1965; Hemenger, 1977b; Knapp, 1984), i.e., the bands in the excitonic spectrum are narrower than in the monomer spectrum. A different situation arises when the monomer spectrum is relatively broad. In that case all excitonic transitions merge into a single band. In the simplest models, each excitonic transition is replaced by a band of a width equal to that of the monomer, i.e., exchange narrowing is ignored. Inhomogeneously broadened excitonic spectra can be simulated by Monte Carlo integration (Fidder et al., 1991; Koolhaas et al., 1994; van Mourik, 1993), whereas theoretical models are available for homogeneously (Hemenger, 1977a; Lagos and Friesner, 1984; Lu and Mukamel, 1991) and lifetime broadened spectra. Except for the last, these models require extensive numerical computations.

The current study

So far, no study includes all of the considerations mentioned above. But such a model would be undesirable, because it would be too complicated to single out the effect of each mechanism. In this paper we develop a global overview of the effects of broadening on excitonic absorption and CD spectra, and discuss new tools that make possible a more quantitative analysis of CD spectra. To do this, we use the simplest model possible for the interaction itself. Unless stated otherwise:

1) Only the dipole-dipole part of the electronic interactions is included in the calculations.

2) Only transition dipole moments are included. Permanent dipole moments are ignored or assumed to contribute only to the dispersive shift of individual pigments.

3) One excited state is included for each pigment. The weak interaction to higher and multiply excited states is not considered here.

4) Dispersive shifts are assumed not to affect the excitonic splitting, but to cause only an overall shift of the excitonic spectrum.

5) In all calculations, the refractive index is assumed to be equal to unity. The actual value in a protein environment is larger, but it is uncertain how much. Whenever necessary, this will be discussed in the accompanying text.

6) Only interactions between neighboring pigments are considered.

In many photosynthetic proteins these assumptions are very reasonable. In other cases the results form a qualitative illustration of spectral properties of the pigment-protein.

Next we summarize excitonic interactions and absorption in pigment complexes. Some tools are introduced, which are necessary to discuss broadened excitonic spectra in the remainder of the text. CD is discussed explicitly in terms of the varying electric field direction. The effects of spectral broadening are investigated next. It is demonstrated that spectral moments (Hemenger, 1977a) reveal important properties of the broadened excitonic spectra and are easy to evaluate. The results are then discussed and illustrated by means of numerically simulated inhomogeneously broadened spectra for a dimer and a hexamer.

Two applications are discussed. The experimental CD spectra of the LH2 light-harvesting complex from purple bacteria are analyzed to distinguish the possible structural organization of subunits within the complex. In addition, the variability that has been observed in the CD spectra of chlorosomes from green bacteria is related to a possible variation in the cylindrical structure of their bacteriochlorophyll *c*-containing subunits.

EXCITONICALLY INTERACTING PIGMENT COMPLEXES

The excitonic state of a pigment complex can be described in the basis $|\Phi_K\rangle$, where each pigment (n) is in one of its eigen states (K_n). These are eigen states of the Hamiltonian H_0 in the absence of interaction. When including interaction, $H = H_0 + V$ and the excitonic states $|\Psi_J\rangle$ can be expressed as a linear combination:

$$H|\Psi_J\rangle = (H_0 + V)|\Psi_J\rangle = E_J|\Psi_J\rangle \quad |\Psi_J\rangle = \sum_K C_{JK}|\Phi_K\rangle. \quad (1)$$

The coefficients C_{JK} and the energies E_J are obtained by diagonalizing the interaction matrix of H on the basis $|\Phi_K\rangle$:

$$\begin{aligned} H_{KL} &= \langle\Phi_K|H|\Phi_L\rangle \\ &= \langle\Phi_K|H_0|\Phi_L\rangle + \langle\Phi_K|V|\Phi_L\rangle \equiv \delta_{KL}W_K + V_{KL}. \end{aligned} \quad (2)$$

In zeroth-order approximation only strongly interacting states (i.e., with $|V_{JK}| > |W_J - W_K|$) need to be included. In particular, for a complex of N identical pigments, we consider only the ground state $|\Phi_0\rangle$ and N singly excited states $|\phi_K\rangle$:

$$\begin{aligned} |\Phi_0\rangle &= \prod_{n=1}^{N} |\phi_n^{(0)}\rangle \qquad W_0 = 0 \\ |\Phi_n\rangle &= |\phi_n^{(k)}\rangle \prod_{m\neq n} |\phi_m^{(0)}\rangle \qquad W_n = w_n^{(k)}, \end{aligned} \quad (3)$$

where $|\Phi_n^{(k)}\rangle$ is the kth excited state of pigment n and $w_n^{(k)}$ is its energy. For convenience we set $w_n^{(0)} = 0$. In the dipole-dipole approximation the interaction operator is expressed in terms of the dipole moment operator ($\tilde{\mu} = \Sigma\tilde{\mu}_n$). Between singly excited states,

$$\begin{aligned} V_{nm} = \langle\Phi_n|V|\Phi_m\rangle &= \frac{\mu_n\cdot\mu_m - 3(\mu_n\cdot\hat{R}_{nm})(\mu_m\cdot\hat{R}_{nm})}{4\pi\varepsilon_0\eta^2R_{nm}^3} \\ &= 5.04\kappa\frac{\|\mu_n\|\,\|\mu_m\|}{\eta^2R_{nm}^3}, \end{aligned} \quad (4)$$

where $\mu_n = \langle\phi_n^{(0)}|\tilde{\mu}_n|\phi_n^{(k)}\rangle$ is the transition dipole moment operator of pigment n, η is the refractive index, R_{nm} is the center-to-center distance between pigments n and m, and $\hat{R}_{nm}$ is the corresponding unit vector. The second equality is correct only if distances are expressed in nanometers, dipole strengths in Debye^2, and the interaction strength in cm^{-1}. To zeroth order, the ground state $|\Phi_0\rangle$ is not perturbed. The singly excited states $|\phi_n\rangle$ are strongly coupled and the excitonic states are determined to zeroth order by diagonalizing the N-dimensional matrix of the Hamiltonian on their basis.

Degenerate dimer

Let us consider the well-known example of a degenerate dimer of pigments with two states: $|\phi_n^{(0)}\rangle$ and $|\phi_n^{(1)}\rangle$, which satisfy $w_1^{(1)} = w_2^{(1)} = w$. The uncoupled dimer has one ground state, $|\Phi_0\rangle = |\phi_1^{(0)}\rangle|\phi_2^{(0)}\rangle$; two singly excited states, $|\Phi_1\rangle = |\phi_1^{(1)}\rangle|\phi_2^{(0)}\rangle$ and $|\Phi_2\rangle = |\phi_1^{(0)}\rangle|\phi_2^{(1)}\rangle$; and one doubly excited state, $|\phi_1^{(1)}\rangle|\phi_2^{(1)}\rangle$. The interaction $V_{12} = V_{21} = \langle\Phi_1|V|\Phi_2\rangle$ strongly couples the singly excited states. In the basis of these two states:

$$H = \begin{bmatrix} w & V_{12} \\ V_{12} & w \end{bmatrix}. \quad (5)$$

This leads to two new excitonic eigenstates: $J = \pm$ with energy levels $E_\pm = w \pm V_{12}$ and

$$\begin{aligned} |\Psi_\pm\rangle &= (|\Phi_1\rangle \pm |\Phi_2\rangle)/\sqrt{2} \\ &= (|\phi_1^{(1)}\rangle|\phi_2^{(0)}\rangle \pm |\phi_1^{(0)}\rangle|\phi_2^{(1)}\rangle)/\sqrt{2}. \end{aligned} \quad (6)$$

Absorption and circular dichroism in excitonic pigment complexes

With the results above, the OD and CD of a pigment complex can be related to the transition dipole moments of the individual pigments. The CD is commonly described with the use of magnetic transition dipole moments (Scherz et al., 1991; Johnson and Tinoco, 1969), which was originally needed to describe the Cotton effect in small molecules (Schellman, 1975). The CD is then expressed in Debye-Bohr magnetons, and for comparison of OD and CD spectra a conversion factor is needed. However, in the case of excitonic interactions it is completely unnecessary to invoke the use of magnetic transition dipole moments. We present a new and straightforward way of calculating the CD, where we consider explicitly the variation of the electric field over the complex, and as a result, no unnecessary conversions have to be made.

Let us first briefly review the mechanism of steady-state light absorption. The electric field component of the light induces an oscillating potential. With linearly polarized light of a wavelength larger than the size of the system, the time-dependent Hamiltonian becomes (II.7)

$$H' = H + H_{OSC}\cos(\omega t) = H + (\bar{E}\cdot\tilde{\mu})\cos(\omega t). \quad (7)$$

Transitions between the ground state $|\Psi_0\rangle$ and excited state $|\Psi_J\rangle$ occur if the frequency matches the energetic difference between them. Following Fermi's golden rule (see, e.g., Atkins, 1983), the transition rate W_{0J} is proportional to the squared transition value of H_{osc}. After averaging over an isotropic sample we obtain

$$\langle W_{0J}\rangle \sim \langle|\langle\Psi_0|H_{OSC}|\Psi_J\rangle|^2\rangle = \langle|\bar{E}\cdot\langle\Psi_0|\tilde{\mu}|\Psi_J\rangle|^2\rangle = \frac{1}{3}E^2\|\mu_J\|^2 \equiv \frac{1}{3}E^2D_J, \quad (8)$$

where μ_J is the transition dipole moment, and E^2 is proportional to the intensity of the light. Apparently the absorption of a molecule is determined by the squared length of its transition dipole moment, also known as dipole strength D_J. For a complex of interacting singly excited states, the transition dipole moment is obtained by applying Eq. 1:

$$\mu_J = \langle\Psi_0|\tilde{\mu}|\Psi_J\rangle = \sum_{n=1}^{N} C_{Jn}\mu_n \qquad D_J = \sum_{n,m=1}^{N} C_{Jn}C_{Jm}(\mu_n\cdot\mu_m). \quad (9)$$

To describe CD we distinguish right and left circularly polarized light. If the light propagates in the positive direction along the z axis, $k = 2\pi\hat{z}/\lambda$, and the electric field component is

$$E^{R/L}(r,t) = \frac{E}{\sqrt{2}}[\cos(\omega t - (k\cdot r))\hat{x} \mp \sin(\omega t - (k\cdot r))\hat{y}] \approx \frac{E}{\sqrt{2}}[\cos(\omega t)(\hat{x} \pm (k\cdot r)\hat{y}) \mp \sin(\omega t)(\hat{y} \mp (k\cdot r)\hat{x})]. \quad (10)$$

The complex is again assumed to be small in relation to the wavelength ($(k\cdot r) \ll 1$). For both polarizations, the transition rate $W_{0J}^{R/L}$ to an excited state is obtained with Fermi's golden rule. This is analogous to Eq. 8, but the oscillating potential is summed over all N pigments at positions r_n:

$$\begin{aligned} W_{0J}^{R/L} &\sim |\langle\Psi_0|H_{OSC}|\Psi_J\rangle|^2 \\ &= \frac{E^2}{2}[\langle\Psi_0|\sum_{n=1}^{N}\hat{x} \pm (k\cdot r_n)\hat{y}\cdot\tilde{\mu}_n|\Psi_J\rangle^2 \\ &\quad + \langle\Psi_0|\sum_{n=1}^{N}\hat{y} \\ &\quad \mp (k\cdot r_n)\hat{x}\cdot\tilde{\mu}_n|\Psi_J\rangle^2] \\ &= E^2\Big[\frac{(\hat{x}\cdot\mu_J)^2 + (\hat{y}\cdot\mu_J)^2}{2} \\ &\quad \mp \frac{2\pi}{\lambda}\sum_{n,m=1}^{N} C_{Jn}C_{Jm}(\hat{z}\cdot r_n)(\hat{z}\cdot\mu_n\times\mu_m)\Big]. \end{aligned} \quad (11)$$

Because the intensity of this light is equal to that of the linearly polarized light in Eq. 8, apparent dipole strengths are obtained by averaging over all orientations of the complex:

$$D_J^{R/L} = D_J \mp \frac{2\pi}{\lambda}\sum_{n,m=1}^{N} C_{Jn}C_{Jm}(r_n\cdot\mu_n\times\mu_m). \quad (12)$$

The average of the two apparent dipole strengths is equal to the dipole strength for linearly polarized light in Eq. 9. The difference is observed as circular dichroism. It is quantitatively expressed by the rotational strength:

$$R_J = \frac{D_J^L - D_J^R}{4} = -\frac{\pi}{2\lambda}\sum_{n,m=1}^{N} C_{Jn}C_{Jm}(r_{nm}\cdot\mu_n\times\mu_m), \quad (13)$$

where $r_{nm} = r_m - r_n$. Note the factor 4 in the definition of rotational strength, which is due to the historical usage of ellipticity as a unit for circular dichroism. In this paper rotational strengths are expressed in units of dipole strength, and circular dichroism is expressed in absorption units. For each band,

$$\frac{CD}{OD} = \frac{A_L - A_R}{A} = \frac{4R_J}{D_J}. \quad (14)$$

The characteristic S-shaped CD spectra discussed below occur by partial overlapping of two or more bands with opposite strengths. Note from Eq. 13 that the CD vanishes in the absence of interaction because only one of the $C_{Jn} \neq 0$. The small amount of CD in monomeric pigments (Cotton effect) is related to their magnetic transitions, which are ignored here.

Degenerate dimer

Using Eq. 6, the transition dipole moments of the two excitonic transitions become

$$\mu_\pm = \frac{\mu_1 \pm \mu_2}{\sqrt{2}} \quad D_\pm = \frac{1}{2}(D_1 + D_2) \pm (\mu_1 \cdot \mu_2). \tag{15}$$

The constant term depends on the dipole strengths of the two pigments, and the variability depends on their relative orientation. Note that the total dipole strength is not affected by the interaction. The rotational strengths are calculated with Eq. 13:

$$R_\pm = \mp \frac{\pi}{2\lambda}(r_{12} \cdot \mu_1 \times \mu_2). \tag{16}$$

BROADENED EXCITONIC SPECTRA AND SPECTRAL MOMENTS

Each absorption transition in a pigment is described by its position (ν_n) and dipole strength (D_n). In the presence of spectral broadening, an additional bandshape function ($\rho(\nu)$) is required, and the transition is replaced by a band $D_k\rho(\nu - \nu_k)$. We assume that all pigments have the same bandshape function. To model the broadening of the excitonic spectra, the excitonic splitting and broadening are to be considered simultaneously. Below we introduce the concept of spectral moments and use it to characterize the excitonic spectrum for a number of broadening mechanisms.

Spectral moments are defined for stick spectra as well as continuous spectra. The former is described by a set of N transitions of strength A_J and energy E_J, and the latter by a function $f(E)$. Their sth spectral moment is defined as

$$A^{[s]} = \sum_{J=1}^{N} A_J E_J^S \tag{17}$$

and

$$f^{[s]} = \int f(E)E^s \, dE.$$

The two definitions are equivalent and apply to absorption as well as circular dichroism. Absorption spectra ($f(E)$) are always positive and behave like distributions. In particular, for the strength and average position of the bands of the uncoupled pigments to match those of the underlying transition, the bandshape function must satisfy $\rho^{[0]} = 1$ and $\rho^{[1]} = 0$. Its main characteristic is its width $\sigma = \sqrt{\rho^{[2]}}$, while $\rho^{[3]}$ represents the asymmetry, and higher moments the detailed bandshape.

Spectral moments are useful because they are easier to calculate than the excitonic spectra themselves. We demonstrate this first for the stick spectra, defined in Eqs. 9 and 13. Both contain products of the form $C_{Jn}C_{Jm}$ for each transition. The spectral moments of such products are

$$\begin{aligned}(C_{Jn}C_{Jm})^{[s]} &= \sum_J C_{Jn}C_{Jm}E_J^S = \sum_J \langle \Phi_n|\Psi_J\rangle\langle\Psi_J|\Phi_m\rangle E_J^S \\ &= \sum_J \langle \Phi_n|H^s|\Psi_J\rangle\langle\Psi_J|\Phi_m\rangle = \langle \Phi_n|H^s|\Phi_m\rangle = (H^s)_{nm}.\end{aligned} \tag{18}$$

This immediately leads to the spectral moments of the stick spectra for absorption as well as circular dichroism:

$$D^{[s]} = \sum_{n,m=1}^{N} (H^s)_{nm}(\mu_n \cdot \mu_m) \equiv \sum_{n,m=1}^{N} (H^s)_{nm}D_{nm} \tag{19}$$

$$R^{[s]} = -\frac{\pi}{2\lambda}\sum_{n,m=1}^{N} (H^s)_{nm}(r_{nm} \cdot \mu_n \times \mu_m) \equiv \sum_{n,m=1}^{N} (H^s)_{nm}R_{nm}.$$

The spectral moments are obtained by summation over all pigment pairs and do not require diagonalization of the interaction matrix.

Convolved excitonic spectra

The simplest way to produce a spectrally broadened excitonic spectrum is obtained by convolving each transition by a band of finite width. Although not based on any concrete mechanism, it may provide a good approximation (Pearlstein, 1991; Scherz et al., 1991), especially when the monomer bands are broad enough to melt all excitonic transitions into a single band. When the bands are narrow, exchange narrowing occurs. This has been demonstrated for the case of inhomogeneous broadening (Hemenger, 1977b; Knapp, 1984), where the bandshape function for each excitonic transition is narrowed by a factor $(\Sigma_{n=1}^{N} C_{Jn}^4)^{-1/2}$ (Knoester, 1993), which for delocalized states ($C_{Jn} \approx N^{-1/2}$) is typically on the order of $N^{1/2}$.

To investigate the validity of the convolution approximation we calculate the spectral moments of the convolved spectrum $f_{con}(\nu) = \Sigma_J A_J \rho(\nu - E_J)$ and compare them to the results for specific broadening mechanisms. These moments can be expressed in terms of those of the stick spectrum (A_J, E_J) and the bandshape function (ρ). It can be shown that

$$\begin{aligned} f_{con}^{[0]} &= A^{[0]} \quad f_{con}^{[1]} = A^{[1]} \quad f_{con}^{[2]} = A^{[2]} + \sigma^2 A^{[0]} \\ f_{con}^{[3]} &= A^{[3]} + 3\sigma^2 A^{[1]} + \rho^{[3]}A^{[0]}. \end{aligned} \tag{20}$$

The first two indicate that the total strength and averaged position of the spectrum are not affected by the convolution, and the second moment is directly related to the fact that the rms (root mean square) bandwidth of the convolved spectrum is equal to the squared sum of the widths of the stick spectrum and the bandshape function.

Inhomogeneously broadened excitonic spectra

This prominent mechanism produces random shifts $\nu_1, \ldots, \nu_N$ in the transitions of each pigment. The stick spectrum is a function of the spectral shifts only, and the broadened spectrum $f_{inh}(\nu)$ is obtained by averaging over the distribution $\rho(\nu_1) \ldots \rho(\nu_N)$. Averaging of the spectral moments can be carried out analytically, because it does not require diagonalization of the interaction matrix. This is discussed in Appendix A, and spectral moments are obtained up to $s = 3$ (see Eqs. 38 and 40):

$$f_{inh}^{[0]} = A^{[0]} \quad f_{inh}^{[1]} = A^{[1]} \quad f_{inh}^{[2]} = A^{[2]} + \sigma^2 A^{[0]}$$
$$f_{inh}^{[3]} = A^{[3]} + \sigma^2(2A^{[1]} + A_0^{[1]}) + \rho^{[3]}A^{[0]}. \tag{21}$$

Up to the second moment, they are equal to those of the convolved excitonic spectrum, which indeed indicates that the latter may be used as an approximation, especially if the broadening is strong ($\sigma > V$). In the expression of the third moment, A_0 is the stick spectrum in the absence of interaction. Its first moment can be normalized to zero.

Note that Eq. 21 includes only uncorrelated spectral shifts. The effects of site correlation (Knoester, 1993) and structural inhomogeneities (Fidder et al., 1991) have been discussed elsewhere.

Homogeneously broadened excitonic spectra

In this case, broadening of the absorption bands is caused by vibrational modes in the pigments as well as coupling to vibrational modes in the protein. Each electronic state splits into a large number of nuclear substates, all of which have to be included in the interaction matrix. Although this inhibits even a numerical diagonalization, the lowest spectral moments can still be obtained because they require only a summation over the entries of the interaction matrix. In Appendix B this is carried out up to $s = 3$. The results are equal to those of the inhomogeneously broadened spectrum (see Eqs. 53 and 56). This indicates that the similarity between them may be larger than with convolution broadened spectra.

Inhomogeneous and homogeneous broadening are both caused by vibrational modes in their protein environment. Slow fluctuations are responsible for inhomogeneous broadening, whereas the faster ones couple into the homogeneous spectrum (Pierce and Boxer, 1992; Stein and Fayer, 1992). In both cases, it is required that the modes be sufficiently localized to be coupled only to one pigment.

Degenerate ground-state theory

In contrast to the case of inhomogeneous broadening, it is not straightforward that even the lowest spectral moments of the homogeneously broadened excitonic spectrum can be expressed in terms of the bandshape function $\rho(\nu)$, because different pigments may have identical monomer absorption spectra but do not necessarily produce identical excitonic spectra. This was previously discussed, for the low temperature limit, up to $s = 4$ (Hemenger, 1977a), but it was stressed that higher spectral moments do depend explicitly on the substates of the pigments and can no longer be expressed in the bandshape function only.

The fact that the main characteristics of the excitonic spectrum are insensitive to the precise nature of the homogeneous broadening led this author to propose the degenerate ground state (DGS) theory. When including only one substate of the electronic ground state, the excitonic spectrum can be evaluated analytically and is identical to the inhomogeneously broadened spectrum.

Until now it has been uncertain whether this result of the DGS theory can be applied at finite temperatures as well. The results in the paragraphs above (and Appendix B) demonstrate, however, that it reproduces the spectral moments correctly up to $s = 3$.

DISCUSSION

Using the spectral moments presented above, we will now discuss the broadened excitonic absorption and circular dichroism spectra themselves. Several questions will be considered: How is a broadened spectrum related to the underlying stick spectrum? Can it be approximated by a convolved or exchange narrowed spectrum? And can we interpret experimental spectra with spectral moments?

Absorption spectra

The lowest moments of convolved and broadened absorption spectra can be calculated with Eqs. 20 and 21, and expressed in terms of the lowest moments of the underlying stick spectrum and the monomeric bandshape function. This is shown in Table 1. It suggests that we can forget how the

TABLE 1 Spectral moments of excitonic absorption spectra

Spectral moment	0th	1st	2nd	3rd
Type	Strength	Position	Width	Asymmetry
Bandshape function ($\rho(\nu)$	1	0	σ^2	$\rho^{[3]}$
Stick spectrum (D_J, E_J)	$D^{[0]}$	$D^{[1]}$	$D^{[2]}$	$D^{[3]}$
(In)homogeneous broadening	$D^{[0]}$	$D^{[1]}$	$D^{[2]} + \sigma^2 D^{[0]}$	$D^{[3]} + 2\sigma^2 D^{[1]} + \rho^{[3]} D^{[0]}$
Convolved stick spectrum	$D^{[0]}$	$D^{[1]}$	$D^{[2]} + \sigma^2 D^{[0]}$	$D^{[3]} + 3\sigma^2 D^{[1]} + \rho^{[3]} D^{[0]}$

stick spectrum was obtained and concentrate only on how it is broadened. The moments of inhomogeneously and homogeneously broadened excitonic spectra are equal up to $s = 3$, although the spectra themselves differ in detail.

The zeroth moment of the broadened spectrum is equal to that of the stick spectrum and thus to the summed dipole strengths of the monomeric pigments (see Eq. 19). This reflects the well-known conservation of dipole strength by excitonic interaction. As far as the broadening is concerned, the first and second moments are equal for convolved and broadened spectra, which implies that the average position and the rms bandwidth are conserved. This is a surprising result because, at first sight, it seems to exclude the possibility of exchange narrowing.

To investigate this apparent discrepancy, and the quality of the convolution approximation, we simulated inhomogeneously broadened spectra of two small pigment complexes: a dimer (d) and ring-shaped hexamer (h). They are shown in Fig. 1, together with convolved, exchange narrowed, and stick spectra. The broadening effects vary when the excitonic splitting is small (1), intermediate (2), or large (3) with respect to the bandwidth. In the first case, the inhomogeneous spectrum differs little from that of the monomer. The limited amount of broadening is reproduced by the convolved stick spectrum and no exchange narrowing occurs.

But in the case of large splitting, the inhomogeneous spectra (d3 and h3) are approximated more accurately by exchange narrowing. The approximation is not so good for the hexamer (h3), because the twofold degeneracy of the underlying transition impairs a perturbative approach.

Most intriguing are the intermediate spectra (d2 and h2), which show more fine structure than both the convolved and exchange narrowed approximation, and are not simply intermediate between the two extremes. This is related to the apparent contradiction between conservation of rms bandwidth and the occurrence of exchange narrowing. The simulated spectra show a limited amount of narrowing, but the resulting loss of bandwidth is compensated by at least two effects. First, part of the dipole strength is redistributed to transitions that are forbidden in the stick spectrum (van Mourik, 1993). Second, the maxima of the inhomogeneous spectrum appear to be shifted with respect to the underlying stick spectrum. This is most clearly seen in the dimer spectrum in d2. It has also been observed in the inhomogeneously broadened spectra of larger ($N = 250$) linear pigment aggregates (Fidder et al., 1991).

These phenomena are not observed with weak (1) or strong (3) interaction. In the former case no exchange narrowing occurs, and in the latter an infinitesimally small redistribution is required. But in typical photosynthetic proteins, where the excitonic splitting is on the same order as the absorption bandwidth, the shape of the excitonic spectra is considerably affected, both by redistribution of dipole strength and broadening-induced shifts. Such spectra may still be simulated with some exchange narrowed convolution, but only if a quantitative expression of these two phenomena is available.

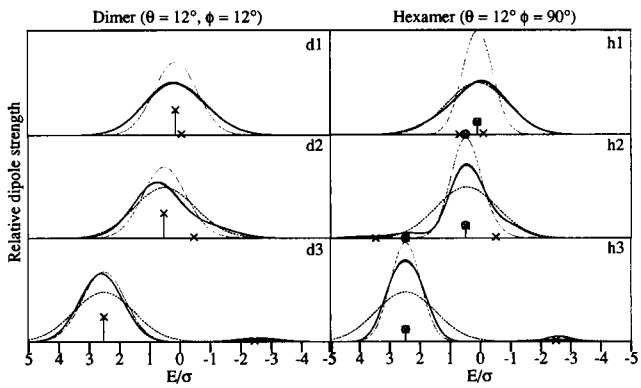

FIGURE 1 Absorption spectra obtained from the stick spectrum by inhomogeneous broadening (——; linewidth indicates rms fluctuation of the Monte Carlo integration), convolution (– – –), and exchange narrowing (·····). The underlying stick spectra are marked with crosses. Additional circles mark the (twofold) degenerate states. From top to bottom are cases of broad (1), intermediate (2), and narrow (3) transitions, obtained by setting the excitonic splitting to $\Delta = \sigma/5$, σ, and 5σ, respectively. Left to right, a dimeric complex in nearly head-tail configuration (d), and a circularly symmetric hexamer with its transition dipole moments along the radius and 12 out of plane (h). The angles θ (with the horizontal plane) and ϕ (with the radius) are defined in Eqs. 26 and 30.

Circular dichroism spectra

The lowest moments of circular dichroism spectra can also be calculated with Eqs. 20 and 21, in combination with Eq. 19, and are shown in Table 2. The zeroth moment is equal to zero for all types of broadening, which reflects the fact that purely excitonic spectra are by definition conservative. In contrast to absorption, a circular dichroism spectrum can be negative as well as positive and cannot be considered as a distribution. As a result, the sth spectral moment is no longer the average value of E^s over the band. In fact, because of the vanishing zeroth moment, the first moment does not change when the spectrum is shifted. Therefore, it is no longer an indication of the average position of the spectrum, but indicates the magnitude of the spectrum instead.

Analogously, the second and third moments are indicators for position and width of the spectrum, respectively.

TABLE 2 Spectral moments of excitonic circular dichroism spectra

Spectral moment	0th	1st	2nd	3rd
Type	—	Strength	Position	Width
Stick spectrum (R_j, E_j)	0	$R^{[1]}$	$R^{[2]}$	$R^{[3]}$
(In)homogeneous broadening	0	$R^{[1]}$	$R^{[2]}$	$R^{[3]} + 2\sigma^2 R^{[1]}$
Convolved spectrum	0	$R^{[1]}$	$R^{[2]}$	$R^{[3]} + 3\sigma^2 R^{[1]}$
Corrected convolution	0	$R^{[1]}$	$R^{[2]}$	$R^{[3]} + 3(\sigma/\varsigma)^2 R^{[1]}$

The differences in the latter demonstrate that the convolved spectrum is broader than the (in)homogeneously broadened spectrum. Therefore we introduce a corrected convolution spectrum by replacing the bandshape function $\rho(\nu)$ by one with a decreased width $\sigma' = \sigma/\varsigma$. The moments of the spectrum thus obtained are shown in the last row of Table 2. By setting $\varsigma^2 = 3/2$, its lowest moments become equal to those of the broadened spectra, and we propose to use this corrected convolution to approximate broadened CD spectra.

To test this assertion, we also simulated inhomogeneously broadened excitonic CD spectra for the systems discussed above. In addition to convolved, exchange narrowed approximations, the corrected convolution spectra are also shown in Fig. 2. The spectra with strong interaction (d3 and h3) show exchange narrowing, just as in the case of absorption. But the spectra with weak interaction (1) are not reproduced by simple convolution. This even underestimates the amplitudes by about 30%. As proposed above, a much better approximation is provided by the corrected convolution spectra.

The redistribution of dipole strengths and broadening-induced shifts that were present in the intermediately broadened absorption spectra are not so pronounced in circular dichroism. Instead, a different phenomenon is observed for the hexamer. Even though the spectra are conservative, the negative lobe has a larger amplitude than the other, because the amount of exchange narrowing differs. This illustrates that asymmetric CD spectra can still be conservative, even in small pigment complexes. In all cases, the corrected convolution provides a better approximation for the spectrum than straightforward convolution.

First moment of circular dichroism

The simple S-shaped spectra in the upper two cases ((1) and (2)) of Fig. 2 are typical for the circular dichroism of small

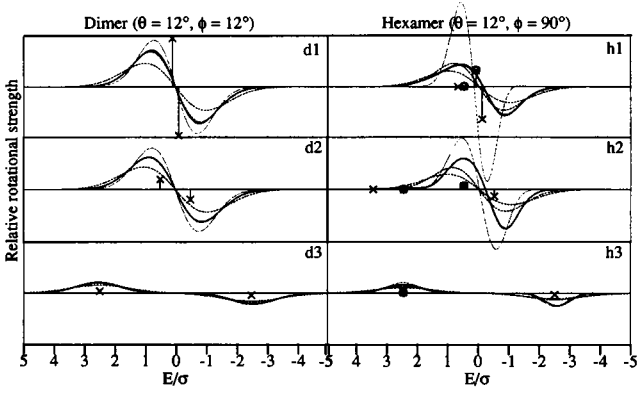

FIGURE 2 Simulated circular dichroism spectra. Models, parameters, and notations are identical to those in Fig. 1, except that the two dashed curves are the convolved and corrected spectrum, respectively (see text). The latter is in all cases narrower and larger. The ordinate axis is scaled with Δ/σ. As a result, the first spectral moments appear equal for broad intermediate and narrow transitions.

pigment-protein complexes. Even the spectra of larger complexes such as chlorosomes (Griebenow et al., 1991), the FMO complex (Pearlstein, 1991), or LHCII (Nussberger et al., 1994) are at least approximately composed of a linear combination of these elementary spectra.

To study such elementary spectra in more detail, note that the weakly (d1) and intermediately (d2) coupled dimer CD spectra of Fig. 2 are remarkably similar, even though the underlying stick spectra are entirely different. In the latter case the rotational strengths are decreased, whereas the excitonic splitting is increased with the same factor. This has little effect on the broadened spectrum, as long as the bandwidth is larger than the excitonic splitting. In that case, the product of rotational strength and excitonic splitting is observed, rather than the two quantities independently. A similar result can be obtained for stick spectra with more than two transitions. In general, the first moment of the rotational strengths ($R^{[1]}$) is the most unambiguous parameter that can be obtained from a CD spectrum.

The correct way to obtain $R^{[1]}$ from experimentally observed CD is by calculating the first moment of the spectrum and applying Eq. 14:

$$\frac{R^{[1]}}{D^{[0]}} = \frac{\mathrm{CD}^{[1]}}{4\mathrm{OD}^{[0]}}. \tag{22}$$

This approach works only for conservative CD spectra, so care should be taken to correct for baseline effects and weak interactions with transitions outside the spectral region of interest. If the latter is equal for all pigments, this correction may be carried out by adding a fraction of the absorption spectrum to the circular dichroism to make it conservative.

The first moment of a simple S-shaped CD spectrum can be obtained with a different approach that avoids these baseline problems. Such spectra occur when the excitonic splitting is smaller than the bandwidth. The CD spectrum is then approximated by convolution of the stick spectrum, including the correction factor (ς). Its shape resembles the first derivative (OD′) of the OD spectrum. Its amplitude is determined by $R^{[1]}$, which can therefore be calculated from three experimentally accessible parameters: the peak-peak amplitude ($\mathrm{CD_{pp}}$) of the circular dichroism, the amplitude of the absorption band ($\mathrm{OD_{max}}$), and its width (full width at half-maximum) (Δ_{FWHM}). By assuming Gaussian absorption bands, it can be shown from Eq. 14 that

$$\frac{R^{[1]}}{D^{[0]}} = \frac{\mathrm{magn(CD)}}{4\varsigma^2\mathrm{magn(OD')}} = \frac{1}{16\varsigma^2}\sqrt{\frac{e}{2\ln 2}}\frac{\Delta_{\mathrm{FWHM}}\mathrm{CD_{pp}}}{\mathrm{OD_{max}}} = 0.058\frac{\Delta_{\mathrm{FWHM}}\mathrm{CD_{pp}}}{\mathrm{OD_{max}}}. \tag{23}$$

The sign of $R^{[1]}$ is determined directly from the shape of the CD spectrum. The right-hand side of Eq. 23 is experimentally accessible, whereas the left-hand side is directly related to the structural model.

Because the first spectral moment of the rotational strengths is independent of the amount of spectral broadening, it is easy to obtain from experimental spectra. Moreover, it has some additional advantages. First, it is obtained by summing the contributions of all pigment-pigment interactions. And second, it is not affected by the energetic site shifts of the interacting pigments. This is an important result because these shifts do occur, are difficult to estimate, and radically influence the shape of the CD spectrum. The first moment is the only tool that can be used to investigate such spectra without assumptions about the site shifts.

EXAMPLES

In this section we apply the tools that we have developed above, particularly the first moment of circular dichroism spectra, to investigate the LH2 light-harvesting antenna from purple bacteria and the chlorosomes from green bacteria.

The LH2 light-harvesting antenna

Most photosynthetic purple bacteria contain LH2 type light-harvesting protein. It occurs in variable amounts around the LH1-RC core particle and absorbs additional light for this particle. The basic subunit of LH2 is formed by a heterogeneous pair of small ($\alpha\beta$) polypeptides and three bacteriochlorophyll pigments. Two strongly interacting pigments absorb at 850 nm and the third one at 800 nm. The LH2 complex is composed of a number (~6-9) of these units. They may be organized as a ring (Zuber and Brunisholz, 1991), as was the case in the recently obtained crystal structure of *Rhodopseudomonas acidophila* LH2 (McDermott et al., 1995). Alternatively, it has been proposed that in *Rhodobacter* (Rb.) *sphaeroides*, the basic spectroscopic building block may be a pair of $\alpha\beta$-subunits (Kramer et al., 1984). These models may be distinguished by means of the B800 pigments. Because these do not interact within the $\alpha\beta$-subunit, all excitonic effects must be due to interaction between units.

Here we consider the LH2 of *Ectothiorhodospira* (Ecto.) sp. Its protein and pigment composition is similar to that of *Rb. sphaeroides*, but its B800 band shows a strong S-shaped circular dichroism spectrum with $CD_{peak\text{-}peak}/OD_{max} = 2.59 \times 10^{-3}$ at room temperature (Ortiz de Zarate et al., manuscript submitted for publication). The corresponding first moment of the rotational strength satisfies $R^{[1]}/D^{[0]} = 0.085\ cm^{-1}$ (see Eq. 23; $\Delta_{FWHM} = 600\ cm^{-1}$). At 77K, the magnitude of the CD increases by a factor of more than 2, but $R^{[1]}$ is hardly affected, which indicates that the structure does not change upon cooling. In addition, the separation between the two extremes of the CD spectrum at this latter temperature implies that the excitonic splitting is less than $130\ cm^{-1}$.

We will investigate whether this strong CD spectrum can be reproduced by excitonic interaction in a (hexameric) ring of B800 pigments, or whether a dimeric organization is required for the pigments and consequently for the $\alpha\beta$-subunits.

Dimer model for LH2

The excitonic absorption and circular dichroism of a degenerate dimer was discussed in above (see Excitonically Interacting Pigment Complexes). Here we calculate the first moment of its rotational strengths directly and include nondegenerate dimers. The two pigments in a dimer are characterized by their positions r_1 and r_2 and transition dipole moments μ_1 and μ_2. On the basis of its two singly excited states the interaction Hamiltonian is expressed as

$$H = \begin{bmatrix} w_1 & V \\ V & w_2 \end{bmatrix}. \tag{24}$$

The first moment of the rotational strengths is obtained with Eq. 19:

$$R^{[1]} = -\frac{\pi}{2\lambda}[V((r_{12} \cdot \mu_1 \times \mu_2) + (r_{21} \cdot \mu_2 \times \mu_1))]$$

$$= -\frac{\pi}{\lambda} V(r_{12} \cdot \mu_1 \times \mu_2), \tag{25}$$

with $r_{12} = r_2 - r_1$. This result agrees with the rotational strengths obtained in Eq. 16. In general, a dimer has three orientational degrees of freedom, which reduce to two by assuming C_2 symmetry:

$$r_{12} = \begin{bmatrix} -d \\ 0 \\ 0 \end{bmatrix} \qquad \mu_1 = \sqrt{D}\begin{bmatrix} \cos\theta\cos\phi \\ \cos\theta\sin\phi \\ \sin\theta \end{bmatrix}$$

$$\mu_2 = \sqrt{D}\begin{bmatrix} -\cos\theta\cos\phi \\ -\cos\theta\sin\phi \\ \sin\theta \end{bmatrix}. \tag{26}$$

Now, by combining Eqs. 25 and 4:

$$\frac{R^{[1]}}{D^{[0]}} = -5.04\frac{\pi}{2}\frac{D}{\lambda d^2}(\cos 2\theta - 3(\cos\theta\cos\phi)^2)\sin 2\theta \sin\phi. \tag{27}$$

Once the leftside is derived from an experimental spectrum, this expression relates d to θ and ϕ. This can be done more concretely by defining a "radius of CD":

$$R_{CD}^2 = 5.04\frac{\pi}{2}\frac{D}{\lambda}\frac{D^{[0]}}{R^{[1]}}. \tag{28}$$

For the B800 CD band of *Ecto. sp.* (D = 39 Debeye^2, λ = 792 nm), R_{CD} = 2.14 nm. Equation 27 reduces to

$$\left(\frac{d}{R_{CD}}\right)^2 = -(\cos 2\theta - 3(\cos\theta\cos\phi)^2)\sin 2\theta \sin\phi. \tag{29}$$

Because the expression on the right side, which we will call the "dimer orientation function," is typically of the order of

unity, the value of RCD is an indication of the pigment-pigment distance. More precisely, the dimer orientation function varies between ±0.58, which produces an upper limit: $d < 1.6$ nm.

By studying the orientation function in more detail, d can be expressed as a function of θ and ϕ. The plot in Fig. 3 is in units of R_{CD} and can therefore be used to analyze the excitonic CD of any C_2-symmetric dimer. The above-mentioned upper limit for d is realized with $\phi = 35°$ and $\theta = 45°$, but this conformation can be excluded, because LD measurements indicate that the out-of-plane angle θ is between 10° and 20° (Ortiz de Zarate et al., manuscript submitted for publication). A new upper limit $d < 1.5$ nm is therefore obtained near the secondary maximum at $\phi = -90°$, $\theta = 22.5°$.

A lower limit for d can also be found because the excitonic splitting ($2V$) is less than 130 cm^{-1} (see above). Considering Eq. 4, and assuming $\kappa > 0.5$, this requires $d > 1.15$ nm. This restricts the possible conformations to the two shaded regions in Fig. 3 (where the assumption for κ is indeed correct).

In principle the two regions can be distinguished by considering the shift between the OD and CD spectrum. The side-by-side orientations in region 1 concentrate the dipole strength in the blue-shifted excitonic transition, whereas the red-shifted state dominates in the head-to-tail of region 2. However, even at 77K, no such shift is observed (Ortiz de Zarate et al., manuscript submitted for publication). There may be two reasons for this. Either the shift is very small, i.e., the splitting is much less than 130 cm^{-1}. In that case an even larger lower limit (than $d > 1.15$ nm) is obtained and thus the conformation must be even closer to the secondary maximum in region 1. Or the transition dipole moments are perpendicular, so that the dipole strength is evenly spread over the two excitonic transitions. This can only be investigated by relaxing the C_2 symmetry condition (Ortiz de Zarate et al., manuscript submitted for publication).

Ring model for LH2

Alternatively, the CD may be caused by excitonic interaction in a ring-shaped arrangement of B800 pigments. In such models, the orientation of one transition dipole moment can be chosen freely (defined by two angles θ and ϕ). All others follow by C_N symmetry around the z axis. For N pigments on a ring with radius r:

$$r_n = r\begin{bmatrix}\cos(\alpha n)\\ \sin(\alpha n)\\ 0\end{bmatrix} \quad \mu_n = \sqrt{D}\begin{bmatrix}\cos\theta\cos(\alpha n+\phi)\\ \cos\theta\sin(\alpha n+\phi)\\ \sin\theta\end{bmatrix}, \tag{30}$$

with $\alpha = 2\pi/N$. For preliminary calculation, we include only nearest-neighbor interactions, and the interaction matrix contains $2N$ entries equal to V; all others are zero. Therefore, with Eq. 19,

$$\frac{R^{[1]}}{D^{[0]}} = -\frac{\pi}{2\lambda}\frac{2NV(r_{12}\cdot\mu_1\times\mu_2)}{ND} = -\frac{\pi}{2\lambda}2V(r_{12}\cdot\hat{\mu}_1\times\hat{\mu}_2)$$

$$\Leftrightarrow \left(\frac{r}{R_{CD}}\right)^2 \tag{31}$$

$$= \frac{(2-\cos^2\theta(2+\cos\alpha-3\cos(2\phi)))\sin 2\theta\sin\phi}{2\sqrt{2(1-\cos\alpha)}}.$$

The value for the "radius of CD" is the same ($R_{CD} = 2.14$ nm) as for the dimer model. The orientation function of the CN complex is plotted in Fig. 4 for the hexamer ($\alpha = 60°$). Its maximum yields an upper limit $r < 2.1$ nm, which is well within the outer radius of 3 nm observed by electron

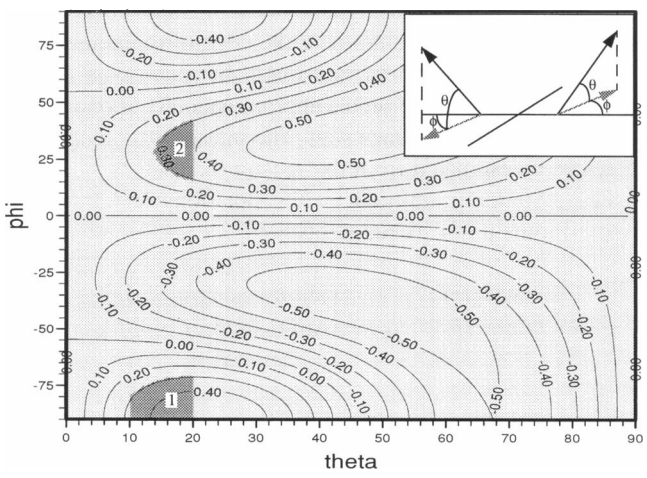

FIGURE 3 Contour plot of the dimer orientation function $(d/R_{CD})^2$ for a C_2 dimer (see Eq. V.6 and text) as a function of the orientation angles θ and ϕ. Maxima: 0.58 ($\phi = 35$, $\theta = 45$) and 0.50 ($\phi = -90$, $\theta = 22.5$). Shaded areas are the possible conformations for a dimeric arrangement of the B800 pigments of Ecto. sp. (see text). The inset illustrates the transition dipole moments of the two pigments and the angles θ and ϕ, as defined in Eq. V.3.

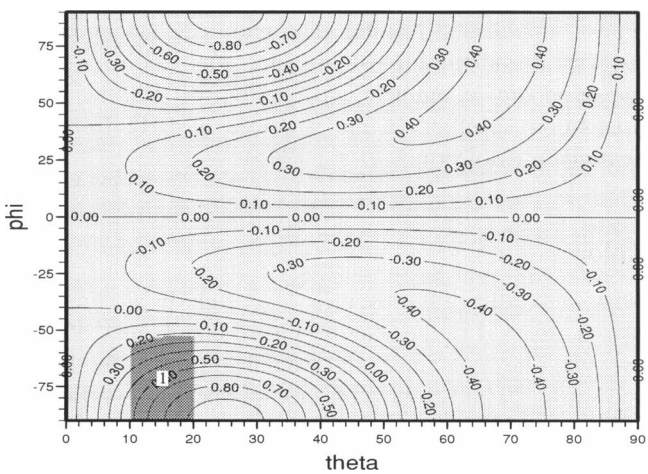

FIGURE 4 Contour plot of the orientation function $(r/R_{CD})^2$ for a C_6 hexamer (see Eq. V.8 and text) as a function of the orientation angles θ and ϕ. Maxima: 0.96 ($\phi = -90$, $\theta = 25$) and 0.50 ($\phi = 90$, $\theta = 71$). Shaded area contains the possible conformations for a hexameric arrangement of the B800 pigments of Ecto. sp. (see text).

microscopy (Boonstra et al., 1993) for LH2 complexes of *Rb. sphaeroides.*

The region of possible conformations of the B800 pigments can be restricted by considering again that $10° < \theta < 20°$, while in view of the size of the pigment molecules, the radius is larger than 1 nm. Therefore, $(r/R_{CD})^2 > 0.22$, which leaves us with the shaded region in Fig. 4, i.e., "tangential" ($-90° < \phi < -54°$). For all of these conformations, the excitonic splitting is below 130 cm^{-1}, which agrees with the experimentally observed CD.

Discussion

The B800 CD of LH2 from *Ecto. sp.* could be explained by excitonic interaction within a ring-shaped hexamer, as well as within a dimer. On the basis of these data alone it is therefore not possible to distinguish between the two organizations by the B800 pigments and consequently by the $\alpha\beta$-subunit of LH2. However, the range of possible models could be considerably restricted. Within the dimer model, the pigment-pigment distance is between 1.15 and 1.5 nm, implying that the coupling is not extremely tight. For a hexameric arrangement, the magnitude of the CD requires that the radius be less than 2.1 nm. For a nonameric arrangement as in LH2 in *Rps. acidophila* (McDermott et al., 1995), the upper limit for the radius becomes 2.6 nm (data not shown). This radius will be slightly larger when nonnearest-neighbor interactions are also taken into account, but in the relatively small rings under consideration, this effect is limited. Therefore, from these calculations we conclude that for a ring-like organization of the B800 pigments in *Ecto. sp.* the radius of the ring is smaller than for the B800 pigments in LH2 from *Rps. acidophila* (3 nm) (McDermott et al., 1995). If the diameter of the ring were to increase, the CD would decrease. In this context it is important to note that the CD of the B800 pigments from LH2 *Rps. acidophila* is indeed smaller (approximately four times; unpublished results). The required "tangential" arrangement and the almost in-plane orientation of the Q_y transition dipole moment are qualitatively similar to the orientation observed in the structure of LH2 from *Rps. acidophila* (McDermott et al., 1995).

Chlorosomes

Next we consider chlorosomes: large light-harvesting complexes attached to the photosynthetic membranes of green bacteria. They contain small amounts of protein and Bchl *a*, and up to 20,000 Bchl *c*, *d*, or *e* pigments, in cylindrical subunits of 5–10 nm diameter (Staehelin et al., 1980). The latter are proposed to be proteinless Bchl aggregates (Krasnovsky and Bystrova, 1980; Smith et al., 1983; Griebenow and Holzwarth, 1990). The Q_y transition is red-shifted with respect to that of the monomeric pigment, e.g., from 660 to 750 nm for the Bchl *c*-containing chlorosomes in *Chlorobium tepidum* (Nozawa et al., 1994). The strong linear dichroism implies that the Q_y transition dipole moments are at an angle of $15 \pm 10°$ with the cylinder axis (van Amerongen et al., 1991; Griebenow et al., 1991). This is in accordance with fluorescence anisotropy and transient absorption (Fetisova et al., 1988; Lin et al., 1991).

The circular dichroism spectra were observed to be strongly variable, even between freshly prepared samples (Griebenow et al., 1991) containing one positive and one or two negative lobes. However, most CD spectra of *Chloroflexus aurantiacus* chlorosomes could be reproduced by a linear combination of two somewhat asymmetric S-shaped basis spectra, which were named type I and II. The zero crossing of the type I spectrum coincides with the absorption maximum while its magnitude varies: $0 < R^{[1]}/D^{[0]} < 0.07$ cm^{-1} (obtained with Eq. 23). The type II spectrum is blue-shifted by approximately 10 nm and is more or less constant ($R^{[1]}/D^{[0]} = -0.02$ cm^{-1}). This variability is not due to differences in preparation (Griebenow et al., 1991), but reflects the presence of two or more structural organizations. However, the absence of changes in absorption and linear dichroism indicates that the differences between these structures are small.

We will demonstrate that the variability of the CD of chlorosomes can be explained by a small variation in the cylindrical structure of its subunits. However, the linear aggregate that is the main structural element of most chlorosome models (see, e.g., Alden et al., 1992) does not give rise to CD. Instead, two detailed cylindrical models have recently been published (Holzwarth and Schaffner, 1994; Nozawa et al., 1994) and will be discussed here. One pigment is included per unit cell, i.e., the environment of each pigment is identical, and we assume that the cylinder is sufficiently long to ignore edge effects. Only Q_y transitions are considered. Strong Q_x-Q_y interactions that could result from the tight packing are absent because of the orientation of the pigments. Finally, because of the tight packing, the interaction strengths cannot be calculated by dipole-dipole approximation. In fact, for typical models (Alden et al., 1992), with the central magnesium near the edge of the neighboring porphyrin rings, the interaction might be much weaker than calculated with a dipole-dipole approximation (LaLonde et al., 1989) and can even change sign. The interaction strength will therefore be estimated from the spectra themselves.

The cylinder is defined by the positions and transition dipole moments of its pigments:

$$r_n = \begin{bmatrix} r\cos(x_n/r) \\ r\sin(x_n/r) \\ d_n \end{bmatrix} \quad \hat{\mu}_n = \begin{bmatrix} \sin\theta\cos(x_n/r + \phi) \\ \sin\theta\sin(x_n/r + \phi) \\ \cos\theta \end{bmatrix}, \qquad (32)$$

where r is the radius of the cylinder, and x_n and d_n are the displacement along the surface and the axis of the cylinder, respectively. The angles θ and ϕ define the transition dipole moment of each pigment relative to its position vector. The excitonic spectra of such cylindrical complexes are derived in Appendix D. Because the interaction strengths depend on the relative positions $V_{nm} = V(m - n)$, the absorption spectrum consists of two sets of transitions near the energies

E_0 and E_1, which are obtained by summing over all local interactions (see Eqs. 62 and 63):

$$E_0 = \sum_n V(n) \tag{33}$$

and

$$E_1 = \sum_n V(n)\cos(x_n/r).$$

The transition dipole moment at E_0 is oriented parallel to the cylinder axis and contains most of the dipole strength. The red shift of the chlorosome absorption spectrum is in line with a dominating effect of negative $V(n)$ values for head-tail-oriented pigments.

The circular dichroism of such a cylindrical aggregate is a sum of two S-shaped spectra. One is formed by two opposite rotational strengths near E_0 and E_1. The second is centered around E_1. Their respective magnitudes are expressed by the two terms in the first moment of the rotational strengths (see Eq. 64):

$$\frac{R^{[1]}}{D^{[0]}} = \frac{\pi}{2}\sum_n V(n)\left(\frac{r}{\lambda}\sin 2\theta \sin\phi\left(1 - \cos\left(\frac{x_n}{r}\right)\right) - \frac{d_n}{\lambda}\sin\left(\frac{x_n}{r}\right)\sin\theta^2\right) \tag{34}$$

$$\approx \frac{\pi}{2}\sum_n V(n)\sin\theta^2\frac{x_n}{r\lambda}(\cot\theta\sin\phi x_n - d_n).$$

The approximation in the second expression is obtained by considering that (for tightly packed chlorophylls) $x_n \ll r =$ 2.5–5 nm for the relevant interactions. The absorption is similar to that of a ring-shaped complex, with two red-shifted states, but the presence of two S-shaped CD components clearly illustrates that the combined properties of ring and helical structures are present in the cylinder.

The occurrence of two independent spectra agrees well with the experimental data. Let us therefore investigate whether the observed variability can be explained by only a minor structural change. This implies that x_n and d_n remain essentially unaltered, whereas the constant LD requires that θ does not change. However, because the dipole moments are nearly parallel to the cylinder axis, ϕ can vary freely, almost without affecting the structure or interaction strengths. The absorption and LD spectra will remain nearly constant, but the CD varies strongly, because of the change in the first term in Eq. 34. This agrees well with the highly variable redmost S-shaped CD component of chlorosomes.

For a quantitative calculation, we consider that pigments with either $x_n = 0$ or $d_n = 0$ do not contribute to the CD and include only the dominant interaction between nearest neighbors diagonally above each other ($d_n = x_n = 0.5$ nm). With $\theta = 15°$, and using the lower limit of $r = 2.5$ nm, the magnitude of the second term ($R^{[1]}/D^{[0]} = 0.02$ cm^{-1}) requires an interaction of $V(n) = -700$ cm^{-1} to this neighbor, which is comparable to the value obtained from a dipole-dipole calculation. If ϕ is now varied between 0° and 90° (or even 180°), the first term in $R^{[1]}/D^{[0]}$ varies between 0 and 0.07 cm^{-1}, exactly equal to the experimentally observed variation. Representative CD spectra are given in Fig. 5. Considering the simple assumptions, the variation is remarkably similar to that of the experimental spectra (Griebenow et al., 1991).

Within the assumptions of this model, an independent estimate of θ can also be obtained. If x_n and d_n are equal, the observed variation of the ratio between the two CD components between 0 and −3.5 implies that cot $\theta = 3.5$ or $\theta = 16°$. This is more or less equal to the experimentally observed value.

In conclusion, we have demonstrated that the observed variability of CD spectra of chlorosomes can be explained with small variations in the structure of the cylindrical subunits that leave the absorption and LD spectra almost unaffected. The models presented here are in agreement with recently proposed cylindrical structures (Holzwarth and Schaffner, 1994; Nozawa et al., 1994). The required change in ϕ can be realized by rotation within the porphyrin plane. A strong interaction was required in the above calculations, but this may be an artifact due to the inclusion of only one interaction. Note that the convergence equation (Eq. 34) is slow because the orientation factor initially increases with the square of the distance.

In the work of Savikhin et al. (1994), no indication for different Bchl *c* spectral forms was observed, which is in agreement with the absence of the need for such distinct spectral forms to describe the steady-state absorption spec-

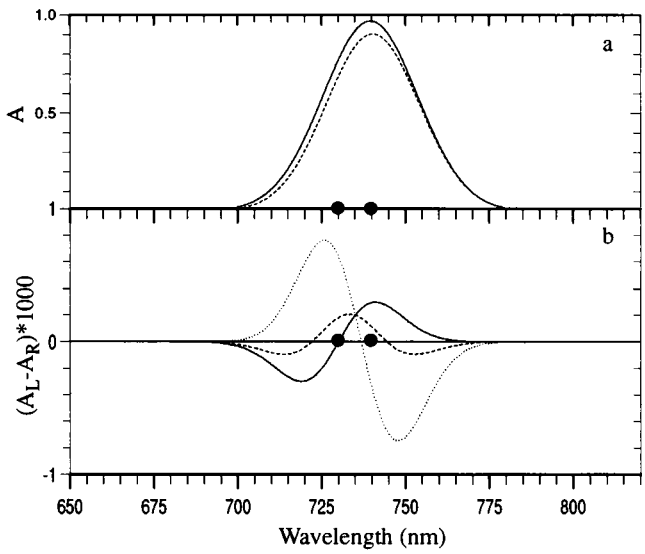

FIGURE 5 Reconstructed chlorosome spectra, based on the analysis in the text. (*a*) Absorption (——) and linear dichroism (– – –) spectrum. (*b*) Circular dichroism of a cylindrical aggregate with $\phi = 0$ (——), $\phi = 16$ (– – –), and $\phi = 90$ (·····). The positions of E_0 (740 nm) and E_1 (730 nm) are marked with a dot on the axis. Other parameters: $\theta = 15°$. $V = -700$ cm^{-1}, $d_n = x_n = 0.5$ nm, $r = 2.5$ nm

tra. The balance between inhomogeneous and homogeneous broadening in chlorosomes is still under debate (Fetisova et al., 1994; Savikhin et al., 1994). However, the present analysis provides a global description of the OD, CD, and LD spectra of cylindrical models and is independent of the type of broadening.

CONCLUSIONS

While investigating the simultaneous occurrence of excitonic interaction and spectral broadening in pigment complexes, we developed several tools to analyze steady-state absorption and circular dichroism spectra of photosynthetic proteins. First we reviewed excitonic interaction in the absence of spectral broadening and described the circular dichroism in terms of the varying electric field direction of circular light over a pigment complex of finite size. This approach is new and has the advantage that it does not require the introduction of magnetic transition dipole moments.

Next we introduced spectral moments, which are readily obtained for inhomogeneously and homogeneously broadened excitonic spectra, and which reveal important properties. In contrast, direct calculation of the actual spectra typically requires lengthy numerical simulation. The integrated magnitude, average position, and root mean square bandwidth of both types of broadened spectra is equal to those obtained by convolving the transitions in the stick spectrum with the bandshape of the uncoupled pigments. This result agrees with the conservation of dipole and rotational strength, but appears to contradict the occurrence of exchange narrowing.

By means of simulated spectra it was illustrated that exchange narrowing occurs only when the interaction strength is larger than the bandwidth. Broad excitonic spectra (i.e., where the bandwidth is larger than the excitonic splitting) can be accurately approximated by the convolution approach, except for CD spectra, the bandshape function of which must be narrowed by a fixed factor $\varsigma = 1.22$ before the stick spectrum is convolved. Consequently, the S-shaped CD spectra that are typically obtained in such cases should be narrower than the first derivative of the corresponding OD spectra. In intermediate cases, a limited amount of exchange narrowing is typically accompanied by a redistribution of absorption strength to forbidden transitions and a shift of the main band.

These results were derived with spectral moments. The higher spectral moments are in principle sensitive to small components at large distances from the main band and do not even converge for Lorentzian bandshapes. Nevertheless, the same results apply to such spectra as long as the main band is not affected by small changes in the peripheral regions.

Our discussion of different broadening mechanisms is by no means complete. As far as inhomogeneous broadening is concerned, we have not yet considered the possibility of correlated spectral shifts (Knoester, 1993) and structural inhomogeneities (Fidder et al., 1991), although it may be possible to include those in the spectral moments.

The effects of dephasing and lifetime broadening were also left out of consideration. Typically, these are described by adding an imaginary component to the energy of each pigment. If this is equal for each pigment, the width of each excitonic band increases by the same amount, and no exchange narrowing occurs. Finally, we considered each pigment with some amount of protein environment as a separate system, and ignored, e.g., the further interaction of excitonic states with their environment. This, among other factors, is responsible for fast inter-exciton state relaxation and may result in considerable additional broadening of particular excitonic states. However, the effects of relaxation are more properly discussed within the density matrix formalism, which is outside the scope of this paper.

The first spectral moment of circular dichroism is a sensitive indicator of its magnitude. We discussed how it can be obtained from experimental spectra, in particular the S-shaped spectra that occur in small pigment complexes, and demonstrated that it can be directly related to the structure of the complex by summing the contributions of individual pigment-pigment interactions. In contrast to the CD spectrum itself, its first moment is independent of the amount of spectral broadening, as well as the dispersive energetic shifts of the pigments that typically result from interactions with the protein matrix.

By means of the first spectral moment, we demonstrated that the strong B800 CD of LH2 from *Ectothiorhodospira sp.* (Ortiz de Zarate et al., manuscript submitted for publication) can be understood with dimeric as well as ring-shaped models, both of which have been proposed for this complex. When a dimeric model is used, the pigment-pigment distance is required to be between 1.15 and 1.5 nm. When a ring-shaped model is used, it is concluded that the Q_y transition dipole moments have an orientation that is "tangential" to the ring, where use has been made of the fact that LD measurements indicate an almost in-plane orientation of the transition dipole moments. This orientation is qualitatively similar to the orientation observed for B800 in the crystal structure of LH2 from *Rps. acidophila* (McDermott et al., 1995). Moreover, it is concluded that the diameter of the B800 ring should be smaller for LH2 from *Ectothiorhodospira sp.* as compared to LH2 from *Rps. acidophila* when a nonameric structure is also assumed.

In addition, it was demonstrated that the experimental variability of the circular dichroism spectra of chlorosomes and the presence of two overlapping S-shaped spectra with independent amplitudes (Griebenow et al., 1991) can be related to the cylindrical organization of its subunits. Although other explanations cannot be excluded, the variability of the CD is elegantly reproduced by small changes in this structure.

All of the results were obtained with a simplified model for the excitonic interaction. Depending on the circumstances, such a model can be used to evaluate the global

characteristics of the excitonic spectra, but refined approaches are available for a more detailed investigation.

APPENDICES

In the first two appendices, we calculate the lowest spectral moments (up to $s = 3$) of inhomogeneously and homogeneously broadened exciton absorption and circular dichroism spectra. We discuss the broadening of known stick spectra (A_J, E_J), defined by a bandshape function $\rho(\nu)$ for the monomer absorption spectra, which we assume to be equal for all pigments.

Appendix A: Spectral moments of inhomogeneous excitonic spectra

As discussed in the text, inhomogeneous broadening results from random spectral shifts of the individual pigments, with a distribution function $\rho(\nu)$. This results in a broadened spectrum of the macroscopic sample. The stick spectrum of each complex is a function of the set $\nu_1, \ldots, \nu_N$ of spectral shifts and is calculated by adding a diagonal matrix $\Delta_{nm} = \delta_{nm}\nu_n$ to the Hamiltonian H. The inhomogeneously broadened excitonic spectrum is obtained by averaging over all N shifts. We denote this by $\langle \ldots \rangle$, i.e., $\langle f \rangle \equiv \int \ldots \int f(\nu_1, \ldots, \nu_N)\rho(\nu_1) \ldots \rho(\nu_N)d\nu_1 \ldots d\nu_N$. The spectral moments of the inhomogeneously broadened spectrum, $f_{inh}(\nu) = \langle \sum_J A_J \delta(\nu - E_J) \rangle$, are obtained by averaging those of the stick spectra (see Eq. 19):

$$f_{inh}^{[s]} = \langle A^{[s]} \rangle = \sum_{n,m=1}^{N} \langle H_{inh}^{s} \rangle_{nm} A_{nm} = \sum_{n,m=1}^{N} \langle (H + \Delta)^s \rangle_{nm} A_{nm}. \tag{35}$$

The factors A_{nm} can represent both D_{nm} (absorption) and R_{nm} (circular dichroism). The diagonal matrix Δ is the only part that actually depends on the ν_n. To facilitate the averaging, we first consider products of the matrices H and Δ:

$$\langle H^r \Delta^s H^t \rangle_{nm} = \left\langle \sum_{l=1}^{N} (H^r)_{nl} \nu_l^s (H^t)_{lm} \right\rangle = \rho^{[s]} (H^{r+t})_{nm} \tag{36}$$

$$\Leftrightarrow \langle H^r \Delta^s H^t \rangle = \rho^{[s]} H^{r+t},$$

for arbitrary r, s, and t. Consequently,

$$\langle (H + \Delta)^0 \rangle = \langle I \rangle = I = H^0$$

$$\langle (H + \Delta)^1 \rangle = \langle H + \Delta \rangle = H^1 \tag{37}$$

$$\langle (H + \Delta)^2 \rangle = \langle H^2 + H\Delta + \Delta H + \Delta^2 \rangle = H^2 + \sigma^2 H^0 .$$

And by finally combining Eqs. 35, 37, and 19:

$$f_{inh}^{[0]} = A^{[0]} \quad f_{inh}^{[1]} = A^{[1]} \quad f_{inh}^{[2]} = A^{[2]} + \sigma^2 A^{[0]}, \tag{38}$$

i.e., up to $s = 2$, the moments of an inhomogeneously broadened exciton spectrum are equal to those of the convolved stick spectrum (in Eq. 20). For evaluation of the third spectral moment, the third power of the Hamiltonian must be averaged. Of the eight terms in that expression, only one cannot be evaluated with Eq. 36:

$$\langle \Delta H \Delta \rangle_{nm} = \langle \nu_n H_{nm} \nu_m \rangle = H_{nm} \delta_{nm} \sigma^2. \tag{39}$$

In contrast to $\langle \Delta^2 H \rangle = \langle H \Delta^2 \rangle = \sigma^2 H$, this product contains only diagonal entries. H can therefore be replaced by the (diagonal) Hamiltonian H_0 of the uncoupled system, including possible dispersive shifts of the individual pigments. The contribution of this term to the summation in Eq. 35 will then contain the first moment of the spectrum of this uncoupled complex, instead of $A^{[1]}$. Thus:

$$\langle (H + \Delta)^3 \rangle = H^3 + \sigma^2(2H + H_0) + \rho^{[3]} H^0 \tag{40}$$

$$\Rightarrow f_{inh}^{[3]} = A^{[3]} + \sigma^2(2A^{[1]} + A_0^{[1]}) + \rho^{[3]} A^{[0]}.$$

The third moment of the inhomogeneously broadened excitonic spectrum is therefore no longer equal to that of a convolved spectrum. The consequences of this difference are discussed in the text. For circular dichroism spectra $A_0^{[1]} = 0$. It can also be normalized to zero for excitonic absorption spectra.

Higher spectral moments can also be obtained, but these contain more mixed products of the form, as in Eq. 39, and depend explicitly on the interactions H_{nm}. This further characterizes the difference between inhomogeneous and convolved excitonic spectra.

Appendix B: Spectral moments of homogeneous excitonic spectra

Homogeneous broadening, as defined in the text, is due to the presence of nuclear substates superimposed on each electronic state. Mixing of all these states in a complex of interacting pigments results in a new set of transitions. We evaluate the lowest moments (up to $s = 3$) of this broadened excitonic spectrum, in three phases. First, the individual pigments are defined. Next, the uncoupled complex is expressed in their basis. Finally, the excitonic coupling is introduced by adding an interaction potential operator to the Hamiltonian. The results can be expressed in terms of the underlying stick spectrum (A_J, E_J) and the bandshape function $\rho(\nu)$ of the monomeric pigments.

The results in this appendix were obtained earlier for the limit of low temperature, with a Green's function approach (Hemenger, 1977a). What is new in this appendix is that we consider all temperatures. Because the spectral moments do not depend on the continuous nature of the spectrum, the results apply for vibrational subbands as well.

Monomeric pigments

Each pigment is defined by a Hamiltonian and a set of eigen states. In addition to the pigment number n and the electronic state k, a third parameter x is needed to denote the nuclear substate. In the Born-Oppenheimer approximation, the eigen states are separated into an electronic and a nuclear part:

$$|\phi_n^{(kx)}\rangle = |\phi_n^{(k)} \chi_n^{(kx)}\rangle \qquad w_n^{(kx)} = w_n^{(k)} + u_n^{(kx)}. \tag{41}$$

Throughout this appendix, identical symbols (e.g., ϕ and w) are used for systems with and without nuclear substates. They can be distinguished by their indices. The separation of the energy level in an electronic ($w_n^{(k)}$) and a nuclear ($u_n^{(kx)}$) component is at this time arbitrary, but becomes clear after Eq. 41. Without affecting the generality of our results, we may assume that the electronic ground-state energies are zero (i.e., $w_n^{(0)} = 0$).

The absorption is determined by the electronic transition dipole moments. In the Born-Oppenheimer approximation,

$$\langle \phi_n^{(0x)} | \tilde{\mu} | \phi_n^{(1y)} \rangle = \langle \phi_n^{(0)} | \tilde{\mu} | \phi_n^{(1)} \rangle \langle \chi_n^{(0x)} | \chi_n^{(1y)} \rangle = \mu_n S_{xy}^n, \tag{42}$$

i.e., the total transition dipole moment μ_n is distributed over the substates, scaled with the Franck-Condon factors $S_{xy}^n = \langle \chi_n^{(0x)} | \chi_n^{(1y)} \rangle$. The basis of nuclear substates is orthonormal and complete:

$$\sum_y S_{xy}^n S_{zy}^n = \sum_y \langle \chi_n^{(0x)} | \chi_n^{(1y)} \rangle \langle \chi_n^{(1y)} | \chi_n^{(0z)} \rangle = \delta_{xz}. \tag{43}$$

The absorption spectrum of the monomeric pigments is finally obtained by considering the fractional thermal population g_x^n of the ground substates $|\phi_n^{(0x)}\rangle$ from which the transitions take place at an energetic shifted $u_{xy}^n =$

$u_n^{(1y)} - u_n^{(0x)}$ with respect to the electronic transition at $w_n^{(1)}$, and with strength $D_n(S_{xy}^n)^2$. This determines the moments of the bandshape function:

$$\rho^{[s]} = \sum_{x,y} g_x^n (u_{xy}^n)^s (S_{xy}^n)^2. \tag{44}$$

Indeed, Eq.43 leads to $\rho^{[0]} = 1$, and $w_n^{(1)}$ can be chosen so that $\rho^{[1]} = 0$.

Uncoupled pigment complex

Only the ground and singly excited states will be considered, in a complex of N pigments:

$$\Phi_G = \prod_{n=1}^{N} \phi_n^{(0G_n)} \qquad W_G = \sum_{n=1}^{N} u_n^{(0G_n)}$$

$$\Phi_{nX} = \phi_n^{(1X_n)} \prod_{m \neq n} \phi_m^{(0X_m)} \tag{45}$$

$$W_{nX} = w_n^{(k)} + u_n^{(1X_n)} + \sum_{m \neq n} u_m^{(0X_m)} \equiv W_n + U_{nX}.$$

The G and X are N-dimensional vectors that contain a substate for each pigment. Note that even a singly excited state includes a ground substate of all other pigments. For computational efficiency in the following, we finally define

$$g_G = \prod_{n=1}^{N} g_{G_n}^n \quad S_{GX}^n = S_{G_nX_n}^n \quad \delta_{GX}^n = \delta_{G_nX_n}. \tag{46}$$

Excitonically coupled complex

The Hamiltonian H ($= H_0 + V$) of the coupled system is obtained by adding the interaction potential operator V to the Hamiltonian H_0 of the uncoupled system. Next, the spectral moments of the homogeneously broadened excitonic spectrum (f_{hom}) are found with Eq. 19. To facilitate the calculations we define a diagonal shift operator:

$$\Delta_{nX,mY} = \delta_{nm}\delta_{XY}U_{nX}. \tag{47}$$

This matrix contains the shift of each substate with respect to its singly excited electronic state. Therefore, the substates become degenerate for the shifted Hamiltonian $H_\Delta = H - \Delta$. The shifts with respect to a particular ground substate G are contained in the diagonal operator $\Delta_G = \Delta - W_G$. With the help of these two additional operators, Eq. 19 can be rewritten. For absorption:

$$f_{hom}^{[s]} = \sum_{G,n,X,m,Y} g_G((H - W_G)^s)_{nX,mY}(\langle\Phi_G|\tilde{\mu}_n|\Phi_{nX}\rangle \cdot \langle\Phi_G|\tilde{\mu}_m|\Phi_{mY}\rangle)$$

$$= \sum_{n,m}\Big[\sum_{G,X,Y} g_G((H_\Delta + \Delta_G)^s)_{nX,mY} S_{GX}^n S_{GY}^m \prod_{p\neq n}\delta_{GX}^p \prod_{q\neq m}\delta_{GY}^q\Big] A_{nm}. \tag{48}$$

The same result is obtained for circular dichroism (with $A_{nm} = R_{nm}$). Because the summation over n and m is familiar from the stick spectra, we first evaluate the summation within the square brackets by dividing $(H_\Delta + \Delta_G)^s$ into separate products. The diagonal of H_Δ contains the electronic excited state energies of the uncoupled pigments, and the off-diagonal entries are formed by the electronic interaction. We assume that these interactions are not affected by the nuclear substates and can be expressed in terms of the $N \times N$ matrix H_{nm} of the electronic states:

$$(H_\Delta^s)_{nX,mY} = \langle\Phi_{nX}|H_\Delta^s|\Phi_{mY}\rangle$$
$$= (H^s)_{nm}(\delta_{nm}\delta_{XY} + (1 - \delta_{nm})S_{YX}^n S_{XY}^m \prod_{p\neq n,m}\delta_{XY}^p). \tag{49}$$

This is simple for $s = 1$ and can be demonstrated by induction for all other values. Furthermore,

$$\sum_{G,X,Y} g_G(\Delta_G^r H_\Delta^s \Delta_G^t)_{nX,mY} S_{GX}^n S_{GY}^m \prod_{p\neq n}\delta_{GX}^p \prod_{q\neq m}\delta_{GY}^q$$

$$= \delta_{nm}(H^s)_{nm}\sum_{G,X_n} g_G (u_{G_nX_n}^n)^{r+t} S_{G_nX_n}^n S_{G_nX_n}^n + (1 - \delta_{nm})$$

$$\cdot (H^s)_{nm}\sum_{G,X_n,Y_m} g_G (u_{G_nX_n}^n)^r (u_{G_mY_m}^m)^t S_{G_nX_n}^n S_{G_mY_m}^m S_{G_nX_n}^m S_{G_mY_m}^m \tag{50}$$

$$= (H^s)_{nm}(\delta_{nm}\rho^{[r+t]} + (1 - \delta_{nm})\rho^{[r]}\rho^{[t]})$$

By substituting $r = s = t = 0$, we find for the zeroth spectral moment,

$$\sum_{G,X,Y} g_G((H_\Delta + \Delta_G)^0)_{nX,mY} S_{GX}^n S_{GY}^m \prod_{p\neq n}\delta_{GX}^p \prod_{q\neq m}\delta_{GY}^q = (H^0)_{nm}, \tag{51}$$

and for the first and second moments,

$$\sum_{G,X,Y} g_G(\Delta_G^0 H_\Delta^1 \Delta_G^0 + \Delta_G^1 H_\Delta^0 \Delta_G^0)_{nX,mY} S_{GX}^n S_{GY}^m \prod_{p\neq n}\delta_{GX}^p \prod_{q\neq m}\delta_{GY}^q = (H^1)_{nm} \tag{52}$$

$$\sum_{G,X,Y} g_G(H_\Delta^2 + H_\Delta\Delta_G + \Delta_G H_\Delta + \Delta_G^2)_{nX,mY} S_{GX}^n S_{GY}^m \prod_{p\neq n}\delta_{GX}^p \prod_{q\neq m}\delta_{GY}^q = (H^2 + \sigma^2 H^0)_{nm}.$$

and insertion of these results into Eq. 48 immediately gives the lowest spectral moments of the homogeneously broadened spectrum:

$$f_{hom}^{[0]} = A^{[0]} \quad f_{hom}^{[1]} = A^{[1]} \quad f_{hom}^{[2]} = A^{[2]} + \sigma^2 A^{[0]}, \tag{53}$$

which is identical to those of the inhomogeneously broadened and convolved stick spectrum (compare Eqs. 38 and 20). It is therefore interesting to consider the third moment to see which of the two will be followed there. One more product must be considered:

$$(H_\Delta\Delta_G H_\Delta)_{nX,mY} = \sum_{l,Z} H_{nl} S_{ZX}^n S_{XZ}^l (U_{lZ} - W_G) H_{lm} S_{YZ}^l S_{ZY}^m \prod_{p\neq n,l}\delta_{XZ}^p \prod_{q\neq l,m}\delta_{YZ}^q. \tag{54}$$

First we evaluate the summation of Eq. 48 with the assumption that the diagonal entries of H are zero:

$$\sum_{G,X,Y} g_G(H_\Delta\Delta_G H_\Delta)_{nX,mY} S_{GX}^n S_{GY}^m \prod_{p\neq n}\delta_{GX}^p \prod_{q\neq m}\delta_{GY}^q = \sum_l H_{nl}H_{lm}$$

$$\Big[\delta_{nm}\sum_{G,X_n,Y_n,Z_n,Z_l} g_G S_{Z_nX_n}^n S_{GlZ_l}^l (u_{GlZ_l}^l + u_n^{(0Z_n)} - u_n^{(0G_n)}) S_{GlZ_l}^l S_{Z_nY_n}^n S_{G_nX_n}^n S_{G_nY_n}^n \tag{55}$$

$$+ (1 - \delta_{nm})\sum_{G,X_n,Y_m,Z_l} g_G S_{G_nX_n}^n S_{GlZ_l}^l u_{GlZ_l}^l S_{GlZ_l}^l S_{G_mY_m}^m S_{G_nX_n}^n S_{G_mY_m}^m\Big]$$

$$= \sum_l H_{nl}H_{lm}\sum_{G,Z} g_G S_{GlZ_l}^l u_{GlZ_l}^l S_{GlZ_l}^l = H_{nm}^2\rho^{[1]} = 0.$$

If the diagonal of H does contain nonzero entries, the terms where l is equal to n or m have to be considered separately. The final result of Eq. 55 does, however, remain equal to zero. With this result, the sum in Eq. 48 can be expressed for $s = 3$:

$$\begin{aligned}
&\sum_{G,X,Y} g_G((H_\Delta + \Delta_G)^s)_{nX,mY} S^n_{GX} S^m_{GY} \prod_{p\neq n} \delta^p_{GX} \prod_{q\neq m} \delta^q_{GY} \\
&= \sum_{G,X,Y} g_G(H^3_\Delta + H^2_\Delta \Delta_G + H_\Delta \Delta_G H_\Delta + \Delta_G H^2_\Delta \\
&+ H_\Delta \Delta^2_G + \Delta_G H_\Delta \Delta_G + \Delta^2_G H_\Delta \qquad (56) \\
&+ \Delta^3_G)_{nX,mY} S^n_{GX} S^m_{GY} \prod_{p\neq n} \delta^p_{GX} \prod_{q\neq m} \delta^q_{GY} \\
&= (H^3 + (2 + \delta_{nm})\sigma^2 H^1 + \rho^{[3]} H^0)_{nm}.
\end{aligned}$$

Finally, the third spectral moment is obtained by substitution:

$$f^{[3]}_{hom} = A^{[3]} + \sigma^2(2A^{[1]} + A^{[1]}_0) + \rho^{[3]} A^{[0]}. \qquad (57)$$

The third moments of the inhomogeneously and homogeneously broadened spectra are equal (see Eq. 40) but differ from that of the convolved spectrum.

Appendix C: Exciton spectral moments of cylinder aggregates

In this appendix we investigate the excitonic absorption and CD spectra of long symmetric cylindrical pigment aggregates. By evaluating the spectral moments, we demonstrate that the absorption contains two main bands and the circular dichroism two "independent" S-shaped spectra. One of these is related to both absorption bands, and the other is centered around one of them. The positions and relative magnitudes depend on the local organization of the pigments. Based on these results, the spectra of circular, helical, and linear aggregates are straightforwardly obtained.

In the considered cylindrical aggregates, all pigments are equivalent, i.e., the unit cell contains only one pigment. Any such complex can be parameterized as a stack of N_2 rings, with N_1 pigments each. Each consecutive ring is rotated by a pitch angle γ_2 with respect to its predecessor. One transition dipole moment may be chosen independently (here in polar coordinates θ and ϕ). All others follow from the symmetry:

$$\begin{aligned}
r_n &= \begin{bmatrix} r\cos(\gamma_1 n_1 + \gamma_2 n_2) \\ r\sin(\gamma_1 n_1 + \gamma_2 n_2) \\ d n_2 \end{bmatrix} \quad \hat{\mu}_n \\
&= \begin{bmatrix} \sin\theta\cos(\gamma_1 n_1 + \gamma_2 n_2 + \phi) \\ \sin\theta\sin(\gamma_1 n_1 + \gamma_2 n_2 + \phi) \\ \cos\theta \end{bmatrix}. \qquad (58)
\end{aligned}$$

where $n = \{n_1, n_2\}$ and $\gamma_1 N_1 = 2\pi$. Alternatively, the position of pigment n may be described by the overall rotation $\alpha_n = \gamma_1 n_1 + \gamma_2 n_2$ or horizontal displacement $x_n = r\alpha_n$ along the surface of the cylinder and the vertical displacement $d_n = d n_2$. Before evaluating the spectral moments with Eq. 19, we first consider that

$$\begin{aligned}
(\hat{\mu}_n \cdot \hat{\mu}_m) &= \cos^2\theta + \sin^2\theta\cos(\alpha_m - \alpha_n) \\
(r_{nm} \cdot \hat{\mu}_n \times \hat{\mu}_m) &= -r\sin 2\theta \sin\phi(1 - \cos(\alpha_m - \alpha_n)) \qquad (59) \\
&\quad - d\sin^2\theta \frac{\partial}{\partial\gamma_2}\cos(\alpha_m - \alpha_n).
\end{aligned}$$

The symmetry of the aggregate is essential for evaluating the summations in Eq. 19. We explain this first for one-dimensional aggregates. The requirements are 1) that the interaction strength depends only on the relative positions $V_{nm} = V(m - n)$, and 2) that the aggregate is periodic or infinitely long. An aggregate of N pigments should satisfy $V(n + N) = V(n)$. Because typically $V_{nm} = V_{mn}$, it follows that for any $\gamma = 2k\pi/N$,

$$\sum_n V_{nm} e^{i\gamma(m-n)} = \sum_n V(n) e^{i\gamma n} = \sum_n V(n)\cos(\gamma n), \qquad (60)$$

independently of m. Moreover, this can be generalized by induction to

$$\begin{aligned}
\sum_n (V^s)_{nm} e^{i\gamma(m-n)} &= \sum_{n,k} (V^{s-1})_{nk} e^{i\gamma(k-n)} V_{km} e^{i\gamma(m-k)} \qquad (61) \\
&= (\sum_n V(n) e^{i\gamma n})^s = (\sum_n V(n)\cos(\gamma n))^s.
\end{aligned}$$

The same result applies for two-dimensional aggregates ($n = \{n_1, n_2\}$ and $\gamma = \{\gamma_1, \gamma_2\}$), as long as these are either periodic or infinitely long in both dimensions. In infinitely long aggregates, the sum is dominated by local interactions. In finite systems, edge effects remove some terms from the summation, but the expression remains correct, as long as the size of the aggregate is larger than the range necessary to obtain convergence of the summation.

With Eq. 59 and the real part of Eq. 61, Eq. 19 can now be evaluated:

$$\begin{aligned}
D^{[s]} &= \sum_{n,m} (V^s)_{nm} D(\cos^2\theta + \sin^2\theta\cos(\alpha_m - \alpha_n)) \qquad (62) \\
&= ND(\cos^2\theta E^s_0 + \sin^2\theta E^s_1),
\end{aligned}$$

where

$$E_0 = \sum_n V(n) \qquad E_1 = \sum_n V(n)\cos(\alpha_n). \qquad (63)$$

Thus the total dipole strength is distributed over two transitions at E_0 and E_1, with relative strengths depending on the angle θ between the transition dipole moments and the cylinder axis. The former is polarized along the cylinder axis and the latter in the plane perpendicular to it. Because there is no preferential direction in this plane, the transition at E_1 is at least twofold degenerate.

For cylinders of finite length, the dipole strength is distributed over a number of transitions near E_0 and E_1. This has little effect on absorption but much more on circular dichroism. For rotational strengths, the combination of Eqs. 19, 59, and 61 yields

$$\begin{aligned}
R^{[s]} &= ND\frac{\pi}{2}\left(\frac{r}{\lambda}\sin 2\theta \sin\phi(E^s_0 - E^s_1) + \frac{d}{\lambda}\sin^2\theta \frac{\partial}{\partial\gamma_2}(E^s_1)\right) \\
&= ND\frac{\pi}{2}\left(\frac{r}{\lambda}\sin 2\theta \sin\phi(E^s_0 - E^s_1)\right. \qquad (64) \\
&\quad \left. - \sum_n \frac{d_n}{\lambda} V(n)\sin(\alpha_n)\sin\theta^2 s E^{s-1}_1\right).
\end{aligned}$$

The partial differentiation with respect to γ_2 refers only to the α_n dependence of E_1 and is factored out on the second line. The first term in Eq. 64 corresponds to a pair of rotational transitions of opposite strength located at E_0 and E_1. The second term may be viewed as a limit of two infinitesimally close transitions with opposite rotational strengths in such a way that the product of their strength and separation is constant. For sufficiently long cylinders, this leads to a single S-shaped spectrum, regardless of the bandwidth. This type of description is analogous to that of electrical

dipoles as a combination of two opposite charges; we might call this a "dipole" spectrum.

Results for circles, helices, and J-aggregates

A number of symmetric subsystems can be distinguished within the cylindrical pigment complex. Their spectra can be derived from that of the cylinder by restricting the interactions. For example, the spectrum of a ring is obtained by setting $V(n_1,n_2) = V'(n_1)\delta_{n2,0}$ so that

$$E_0 = 2V \quad E_1 = \sum_{n_1} V'(n_1)\cos(\gamma_1 n_1)$$

$$D^{[s]} = ND(\cos^2\theta E_0^s + \sin\theta^2 E_1^s) \tag{65}$$

$$R^{[s]} = ND\frac{\pi}{2}\frac{r}{\lambda}\sin 2\theta \sin\phi(E_0^s - E_1^s),$$

which is identical to the result obtained directly in Eq. 31. The obvious difference with the cylinder is the loss of the second type of CD. Only one S-shaped spectrum is observed in this type of aggregate.

Alternatively, a helix is created by including only $V(n_1,n_2) = V'(n_2)\delta_{n1,0}$:

$$E_0 = 2V \quad E_1 = \sum_{n_2} V'(n_2)\cos(\gamma_2 n_2)$$

$$D^{[s]} = ND(\cos^2\theta E_0^s + \sin\theta^2 E_1^s) \tag{66}$$

$$R^{[s]} = ND\frac{\pi}{2}\left(\frac{r}{\lambda}\sin 2\theta \sin\phi(E_0^s - E_1^s) - \frac{d}{\lambda}2V\sin\gamma_2 \sin^2\theta\, sE_1^{s-1}\right).$$

In this aggregate both types of circular dichroism are present again. However, for a linear helix with all pigments on the axis ($r = 0$),

$$R^{[s]} = ND\frac{\pi}{2}\left(-\frac{d}{\lambda}2V\sin\gamma_2 \sin^2\theta\, sE_1^{s-1}\right), \tag{67}$$

and thus the first type of CD is lost. Therefore, the first type of CD may be named "circular CD," and the second type is "helical CD."

Finally, a linear aggregate is created by orienting all pigments parallel ($\gamma_2 = 0$):

$$E_0 = E_1 = 2V$$

$$D^{[s]} = NDE_0^s \qquad R^{[s]} = 0, \tag{68}$$

with only a single shifted excitonic transition, without circular dichroism.

The authors thank Drs. Gert van der Zwan, Walter S. Struve, Leonas Valkunas, and Frank van Mourik for their valuable discussion of the manuscript.

This work was financially supported by the Dutch Organization for Scientific Research (NWO), the Foundation for Life Sciences (SLW), EC contract 92-0796, and NATO contract 940851.

REFERENCES

Alden, R. G., S. H., Lin, and R. E. Blankenship. 1992. Theory of spectroscopy and energy transfer of oligomeric pigments in chlorosome antennas of green photosynthetic bacteria. *J. Lumin.* 51:51–66.

Atkins, P. W. 1983. Molecular Quantum Mechanics. Oxford University Press, New York. 187–199.

Barzda, V., L. Mustardy, and G. Garab. 1994. Size dependency of circular dichroism in macroaggregates of photosynthetic pigment-protein complexes. *Biochemistry.* 33:10837–10841.

Becker, M., V. Nagarajan, and W. W. Parson. 1991. Properties of excited singlet states of bacteriochlorophyll *a* and bacteriopheophytin *a* in polar solvents. *J. Am. Chem. Soc.* 113:6840–6848.

Boonstra, A. F., R. W. Visschers, F. Calkoen, R. van Grondelle, E. F. J. van Bruggen, and E. J. Boekema. 1993. Structural characterization of the B800–850 and B875 light-harvesting antenna complexes from *Rhodobacter sphaeroides* by electron microscopy. *Biochim. Biophys. Acta.* 1142:181–188.

Cogdell, R. J., and H. Scheer. 1985. Circular dichroism of light-harvesting complexes from purple photosynthetic bacteria. *Photochem. Photobiol.* 42:669–689.

de Boer, S., and D. A. Wiersma. 1989. Optical dynamics of exciton and polaron formation in molecular aggregates. *Chem. Phys.* 131:135–144.

Fetisova, Z. G., A. M. Freiberg, and K. E. Timpmann. 1988. Long-range molecular order as an efficient strategy for light harvesting in photosynthesis. *Nature.* 334:633–634.

Fetisova, Z. G., K. Mauring, and A. S. Taisova. 1994. Strongly exciton-coupled BChl *e* chromophore system in the chlorosomal antenna of intact cells of the green bacterium *Chlorobium phaeovibrioides*: a spectral hole burning study. *Photosynth. Res.* 41:205–210.

Fidder, H., J. Knoester, and D. A. Wiersma. 1991. Optical properties of disordered molecular aggregates: a numerical study. *J. Chem. Phys.* 95:7880–7890.

Förster, Th. 1965. Delocalized excitation and excitation transfer. *In* Modern Quantum Chemistry, III. Action of Light and Organic Crystals. O. Sinanoglu, editor. Academic Press, New York. 93–137.

Griebenow, K., and A. R. Holzwarth. 1990. *In* Molecular Biology of Membrane-Bound Complexes in Phototropic Bacteria. G. Drews and E. A. Dawes, editors. Plenum, London. 375–381.

Griebenow, K., A. R. Holzwarth, F. van Mourik, and R. van Grondelle. 1991. Pigment organization and energy transfer in green bacteria. 2. Circular and linear dichroism spectra of protein-containing and protein-free chlorosomes isolated from *Chloroflexus aurantiacus* strain Ok-70-fl. *Biochim. Biophys. Acta.* 1058:194–202.

Hemenger, R. P. 1977a. A theory of optical absorption by aggregates of large molecules. *J. Chem. Phys.* 66:1795–1801.

Hemenger, R. P. 1977b. Optical spectra of molecular aggregates near the strong coupling limit. *J. Chem. Phys.* 67:262–264.

Holzwarth, A. R., and K. Schaffner. 1994. On the structure of bacteriochlorophyll molecular aggregates in the chlorosomes of green bacteria. A molecular modelling study. *Photosynth. Res.* 41:225–233.

Jankowiak, R., J. M. Hayes, and G. J. Small. 1993. Spectral hole-burning spectroscopy in amorphous molecular solids and proteins. *Chem. Rev.* 93:1471–1502.

Johnson, W. C., Jr., and I. Tinoco, Jr. 1969. *Biopolymers.* 7:727.

Keller, D., and C. Bustamante. 1986a. Theory of the interaction of light with large inhomogeneous molecular aggregates. I. Absorption. *J. Chem. Phys.* 84:2961–2971.

Keller, D., and C. Bustamante. 1986b. Theory of the interaction of light with large inhomogeneous molecular aggregates. II. Psi-type circular dichroism. *J. Chem. Phys.* 84:2972–2980.

Knapp, E. W. 1984. Lineshapes of molecular aggregates. Exchange narrowing and intersite correlation. *J. Chem. Phys.* 85:73–82.

Knoester, J. 1993. Nonlinear optical line shapes of disordered molecular aggregates: motional narrowing and the effect of intersite correlations. *J. Chem. Phys.* 99:8466–8479.

Koolhaas, M. H. C., F. van Mourik, G. van der Zwan, and R. van Grondelle. 1994. The B820 sub-unit of the bacterial light-harvesting antenna, a dis-ordered dimer? *J. Lumin.* 60 and 61:515–519.

Kramer, H. J. M., R. van Grondelle, C. N. Hunter, W. H. J. Westerhuis, and J. Amesz. 1984. Pigment organization of the B800–850 antenna complex of *Rhodopseudomonas sphaeroides. Biochim. Biophys. Acta.* 765: 156–165.

Krasnovsky, A. A., and M. I. Bystrova. 1980. Self-assembly of chlorophyll aggregated structures. *BioSystems.* 12:181–194.

Lagos, R. E., and R. Friesner. 1984. Calculation of optical lineshapes for generalized multilevel systems. *J. Chem. Phys.* 81:5899–5905.

LaLonde, D. E., J. D. Petke, and G. M. Maggiora. 1988. Evaluation of approximations in molecular exciton theory. 1. Applications to dimeric systems of interest in photosynthesis. *J. Phys. Chem.* 92:4746–4752.

LaLonde, D. E., J. D. Petke, and G. M. Maggiora. 1989. Evaluation of approximations in molecular exciton theory. 2. Applications to oligomeric systems of interest in photosynthesis. *J. Phys. Chem.* 93:608–614.

Lin, S., H. van Amerongen, and W. S. Struve. 1991. Ultrafast pump-probe spectroscopy of bacteriochlorophyll *c* antenna in bacteriochlorophyll *a* containing chlorosomes from the green photosynthetic bacterium *Chloroflexus aurantiacus. Biochim. Biophys. Acta.* 1060:13–24.

Lu, N., and S. Mukamel. 1991. Polaron and size effects in optical lineshapes of molecular aggregates. *J. Chem. Phys.* 95:1588–1607.

McDermott, G., S. M. Prince, A. A. Freer, A. M. Hawthornthwaite-Lawless, M. Z. Papiz, R. J. Cogdell, and N. W. Isaacs. 1995. Crystal structure of an integral membrane light-harvesting complex from photosynthetic bacteria. *Nature.* 374:517–521.

Myeong-Hee, K., L. Ulibarri, D. Keller, M. F. Maestre, and C. Bustamante. 1986. Theory of the interaction of light with large inhomogeneous molecular aggregates. III. Calculations. *J. Chem. Phys.* 84:2981–2989.

Nozawa, T., K. Ohtomo, M. Suzuki, H. Nakagawa, Y. Shikama, H. Konami, and Z.-Y. Wang. 1994. Structures of chlorosomes and aggregated Bchl *c* in *Chlorobium tepidum* from solid state high resolution CP/MAS 13C NMR. *Photosynth. Res.* 41:211–223.

Nuijs, A. M., R. van Grondelle, H. L. P. Joppe, A. C. van Bochove, and L. N. M. Duysens. 1985. Singlet and triplet excited carotenoid and antenna bacteriochlorophyll of the purple bacterium *Rhodospirillum rubrum* as studied by picosecond absorbance difference spectroscopy. *Biochim. Biophys. Acta.* 810:94–105.

Nussberger, S., J. P. Dekker, W. Kuhlbrandt, B. M. van Bolhuis, R. van Grondelle, and H. van Amerongen. 1994. Spectroscopic characterization of three different monomeric forms of the main chlorophyll a/b binding protein from chloroplast membranes. *Biochemistry.* 33:14775–14783.

Pearlstein, R. M. 1991. Theoretical interpretation of antenna spectra. *In* Chlorophylls. H. Scheer, editor. CRC Press, Boca Raton, FL. 1047–1078.

Pearlstein, R. M., and R. P. Hemenger. 1978. Bacteriochlorophyll electronic transition moment directions in bacteriochlorophyll *a* protein. *Proc. Natl. Acad. Sci. USA.* 75:4920–4929.

Philipson, K. D., and K. Sauer. 1972. Exciton interaction in a bacteriochlorophyll-protein from chloropseudomonas ethylica. Absorption and circular dichroism at 77K. *Biochemistry.* 11:1880–1885.

Pierce, D. W., and S. G. Boxer. 1992. Dielectric relaxation in a protein matrix. *J. Phys. Chem.* 96:5560–5566.

Savikhin, S., Y. Zhu, S. Lin, R. E. Blankenship, and W. S. Struve. 1994. Femtosecond spectroscopy of chlorosome antennas from the green photosynthetic bacterium *Chloroflexus aurantiacus. J. Phys. Chem.* 98: 10322–10334.

Schellman, J. A. 1975. Circular dichroism and optical rotation. *Chem. Rev.* 75:323–331.

Scherz, A., V. Rosenbach-Belkin, and J. R. E. Fisher. 1991. Chlorophyll aggregates in aqueous solutions. *In* Chlorophylls. H. Scheer, editor. CRC Press, Boca Raton, FL. 237–268.

Schreiber, M., and Y. Toyozawa. 1982. Numerical experiments on the absorption lineshape of the exciton under lattice vibrations. II. Average oscillator strength per state. *J. Phys. Soc. Jpn.* 51:1537–1543.

Smith, K. M., L. A. Kehres, and J. Fajer. 1983. Aggregation of the bacteriochlorophylls c, d and e. Models for the antenna chlorophylls of green and brown photosynthetic bacteria. *J. Am. Chem. Soc.* 105: 1387–1389.

Staehelin, L. A., J. R. Golecki, and G. Drews. 1980. Supramolecular organization of chlorosomes (*Chlorobium* vesicles) and of their membrane attachment sites in *Chlorobium limicola. Biochim. Biophys. Acta.* 589:30–45.

Stein, A. D., and M. D. Fayer. 1992. Spectral diffusion in liquids. *J. Chem. Phys.* 97:2948–2962.

van Amerongen, H., B. van Haeringen, M. van Gurp, and R. van Grondelle. 1991. Polarized fluorescence measurements on ordered photosynthetic antenna complexes: chlorosomes of *Chloroflexus aurantiacus* and B800–850 antenna complexes of *Rhodobacter sphaeroides. Biophys. J.* 59:992–1001.

van Mourik, F. 1993. Spectral inhomogeneity of the bacterial light-harvesting antennae: causes and consequences. Ph.D. thesis. Free University Amsterdam, The Netherlands. 21–26.

van Mourik, F., J. R. van der Oord, K. J. Visscher, P. S. Parkes-Loach, P. A. Loach, R. W. Visschers, and R. van Grondelle. 1991. Exciton interaction in the light-harvesting antenna of photosynthetic bacteria studied with triplet-singlet spectroscopy and singlet-triplet annihilation on the B820 subunit form of *Rhodospirillum rubrum. Biochim. Biophys. Acta.* 1059:111–119.

Visschers, R. W., M. C. Chang, F. van Mourik, P. S. Parkes-Loach, B. A. Heller, P. A. Loach, and R. van Grondelle. 1991. Fluorescence polarization and low-temperature absorption spectroscopy of a subunit form of light-harvesting complex I from purple photosynthetic bacteria. *Biochemistry.* 30:2951–2960.

Warshel, A., and W. W. Parson. 1987. Spectroscopic properties of photosynthetic reaction centers. 1. Theory. *J. Am. Chem. Soc.* 109:6143–6152.

Zuber, H., and R. A. Brunisholz. 1991. Structure and function of antenna polypeptides and chlorophyll-protein complexes: principles and variability. *In* Chlorophylls. H. Scheer, editor. CRC Press, Boca Raton, FL. 627–719.